IEEE Access
Multidisciplinary | Rapid Review | Open Access Journal

Received July 21, 2019, accepted August 13, 2019, date of publication August 19, 2019, date of current version September 5, 2019.

Digital Object Identifier 10.1109/ACCESS.2019.2936184

A Low-Cost System for Seismocardiography-Based Cardiac Triggering: A Practical Solution for Cardiovascular Magnetic Resonance Imaging at 3 Tesla

RADEK MARTINEK[1], JINDRICH BRABLIK[1], JAKUB KOLARIK[1], MARTINA LADROVA[1], JAN NEDOMA[2], RENE JAROS[1], LUKAS SOUSTEK[1], RADANA KAHANKOVA[1], MARCEL FAJKUS[1], LUBOMIR VOJTISEK[3], PAVLA HANZLIKOVA[4], AND PETR KRUPA[4]

[1]Department of Cybernetics and Biomedical Engineering, Faculty of Electrical Engineering and Computer Science, VSB-Technical University of Ostrava, 708 00 Ostrava, Czech Republic
[2]Department of Telecommunications, Faculty of Electrical Engineering and Computer Science, VSB-Technical University of Ostrava, 708 00 Ostrava, Czech Republic
[3]Neuroscience Centre, Central European Institute of Technology (CEITEC), Masaryk University, 601 77 Brno, Czech Republic
[4]Department of Imaging Method, Faculty of Medicine, University of Ostrava, 703 00 Ostrava, Czech Republic

Corresponding author: Radek Martinek (radek.martinek@vsb.cz)

This work was supported in part by the Ministry of Education of the Czech Republic under Project SP2019/85 and Project SP2019/118, in part by the European Regional Development Fund in the Research Centre of Advanced Mechatronic Systems Project under the Operational Programme Research, Development and Education under Project CZ.02.1.01/0.0/0.0/16_019/0000867, in part by the Grant Programme Support for Science and Research in the Moravia-Silesia Region 2018 through the Budget of the Moravian-Silesian Region under Grant RRC/10/2018, and in part by the Core Facility MAFIL of CEITEC, MEYS, Czech-BioImaging, under Grant CR LM2015062.

ABSTRACT This study describes a pilot clinical validation of a new low-cost system for the continuous monitoring of the human body's cardiorespiratory activities within the magnetic resonance examination area. This study primarily focuses on monitoring cardiac activity and the related cardiac triggering. The patented system tested by the authors is based on seismocardiography (SCG). The study was conducted on 18 subjects on a Siemens Prisma 3T MR scanner. Standard anatomical and diffusion sequences were used to test cardiac activity monitoring. A wide range of commonly used diagnostic sequences were used to test imaging of the heart by means of cardiac triggering. System functionality was verified against a commercially available electrocardiography (ECG) system. Monitoring of cardiac activity (detection of the R-R interval in ECG and the AO-AO interval in SCG) was objectively evaluated by determining the overall probability of correct detection (ACC), sensitivity (SE), positive predictive value (PPV), and harmonic mean between SE and PPV, i.e. F1. Imaging quality control using Cardiac Triggering was performed by subjective evaluation of images by the physicians. The study conducted clearly confirmed the functionality of the system in terms of continuous cardiac activity monitoring. In all 18 subjects, a mean PPV > 99 % was achieved; F1 > 99 %; SE > 99 %; ACC > 98 %; $1.96\sigma < 3.5$ bpm. Also, Cardiac Triggering functionality was confirmed by the physicians on the basis of analyzing cardiac images using the T1/T2 balanced echo sequences and the T1 flash sequence measured natively.

INDEX TERMS Seismocardiography-based cardiac triggering, seismocardiography (SCG), siemens prisma 3T, monitor patient vital signs during MRI, cardiac magnetic resonance imaging (CMRI).

I. INTRODUCTION

Cardiac magnetic resonance imaging (CMRI) examination is important in the diagnosis of ischemic or inflammatory diseases [1]–[3]. This method also enables distinguishing between reversible and irreversible myocardial changes and detecting small areas of myocardial fibrosis or inflammation. Classification of MR signal changes allows monitoring of the disease process at the tissue level, which is of clinical relevance for non-invasive disease management. Early and

The associate editor coordinating the review of this article and approving it for publication was Yue Zhang.

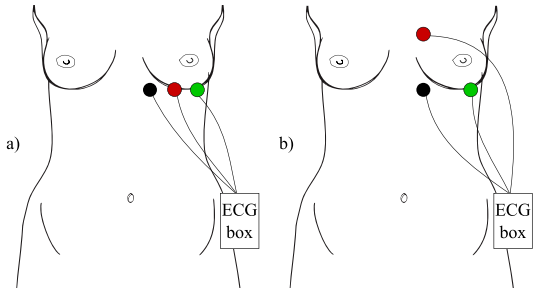

FIGURE 1. Typical arrangement of ECG electrodes in an MRI environment; a) arrangement advantageous for ultra-high magnetic fields and b) arrangement at field strengths of 1.5 T.

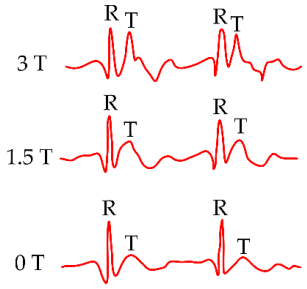

FIGURE 2. Changes in the ECG signal morphology caused by various magnetic fields.

robust detection of scarring or inflammatory myocardial infiltration may allow treatment procedures to be adapted to prevent or delay disease progression. Another application of CMRI is to monitor left ventricle function and dysfunction both in diagnosing local disorders and in diagnosing global hypofunction, which is an important indicator of many heart diseases such as coronary artery disease, myocardial infiltration with inflammatory cells or metabolic products, various types of cardiomyopathy, changes during diabetes or hypertension [4], [5].

The synchronization by the methods of triggering and gating is used in the practice for the insuring of the satisfactory quality of the heart's image. These techniques are essential for the improvement of the image's temporal and spatial resolution. The synchronization is based on the cardiac and respiratory activity monitoring, according to which the CMRI acquisition is triggered. The goal is to minimize the negative effect of the heart and thorax motion on the resulting scan. One of the examples of those artefacts in the image are so-called ghosts manifesting as the shadows in the MRI image [6]. The triggering principle is based on the detection of the most significant change in the electrical signal (e.g. the R wave in ECG signal) as a reflection of the initiation of ventricular depolarization and contraction (ventricular systole). The R wave is referred to as the beginning of the ECG signal period. For the successful peak detection and consecutive synchronization, the task of ECG measurement for the purpose of MRI triggering is to obtain the most distinct R wave and a negative or straight T wave, which can be achieved by changing the electrode arrangement, see Fig. 1 [7]–[10].

The ECG measuring is a means of quick recording of the cardiac function from which every phase of the cardiac cycle applicable to MRI triggering can be read. However, when measured in an MRI device and its magnetic field, many problems exist, such as artifacts arising from inhomogeneity of the magnetic field caused by the patients themselves or foreign materials [11].

For the best possible prevention of artifacts, the skin needs to be well prepared at the locations of the ECG electrodes in order to ensure an optimal electrode-to-skin-contact and minimal skin impedance which helps with the proper triggering during CMRI examinations [12], [13]. Hair must be shaved immediately prior to the examination and the skin surface must be scrubbed with mild abrasive soap or gel before the electrodes are applied, thus making the examination relatively complicated and uncomfortable for the patient [6].

Because of the interaction of the ECG system with radiofrequency and gradient systems, some security steps are important for the ECG sensing – ECG, as a measurement with the electrically active components, brings a risk of surface heating of the patient's skin, or even burns resulting from high voltage induction in ECG hardware [14], [15]. For the prevention of the occurrence of the currents in ECG leads due to the fast switching of the gradient fields, the location of the leads is designed that loops in the cables are not present and the wires are as short as possible [6]. The wires are placed out of resonators for the reducing of the possibility of burns due to interaction with the RF field [11].

Another important complication in ECG synchronization is so-called magnetohydrodynamic effect caused by the MR scanner's magnetic field, which brings the distortion of the ST segment of ECG signal. The ECG triggering is not suitable for the use in the ultra-high magnetic fields, when the effect of this artifact is increasing – at an intensity higher than 3T, the recording is significantly distorted in both the spatial and temporal domains to the extent that the R wave is not unambiguously determined because the magnitude of the T wave equals or exceeds the R wave maxima, see Fig. 2 [16]–[18]. The amplitude of T wave can exceed the R wave for 20 % of its amplitude, i.e. the amplitude increases on 315 % of the original T wave magnitude, even with using of the 1.5 T field intensity [19]. These effects on T and R waves can result in magnetic scanner startup problems (prolonging the scan time leading to the economic loss) because R wave is detected incorrectly, especially at higher magnetic fields (3T and 7T), see [20], [21].

In this study, pilot clinical verification of a new type of a seismocardiography based measurement system (SCG) patented by the authors is presented. This system addresses a number of the above-mentioned problems of a conventionally used ECG-based system. Based on the physicians' experience, ECG-based systems can be considered as the most accurate and reliable system used for triggering in clinical practice. For this reason, the results of this study are verified using the commercial ECG BRAINVISION – BrainAmp

TABLE 1. Baseline characteristics of the volunteers.

Name	(N = 18)
Age, years	37±16
Females, n (%)	8 (44)
Height, cm	171±17
Weight, kg	79±30
BMI, kg/m^2	25.4±2.5
Systolic blood pressure, mmHg	121±22
Diastolic blood pressure, mmHg	73±14

ExG system by BRAIN Product [22]–[24]. Thus, this study primarily focuses on measuring cardiac activity.

The original benefit of this article is clinical verification of functionality of a new cardiac monitoring system, which is necessary for cardiac triggering. The study was conducted on 18 subjects at a Siemens Prisma 3T MR Scanner [25], [26] within a multimodal and functional imaging laboratory (CEITEC [27] Research Centre on Life Sciences, Advanced Materials and Technologies), see [28].

The measurements were conducted on a sample of 18 healthy persons (volunteers) upon their written consent. The age group of the volunteers was from 21 to 53 years and their weight was from 49 to 109 kg. The group of volunteers consisted of 10 men and 4 women. Table 1 presents the baseline characteristics of the study volunteers.

To test the cardiac activity monitoring, we used following types of sequences:

- Standard anatomical sequences
  - T1 mprage,
  - T2_spc_T2_spc _FLAIR,
- fmri (epi_bold) and diffusion sequences,
- Additional research pulse sequences:
  - mp2rage,
  - diffusion and functional imaging sequences using parallel layer excitation, i.e. simultaneous multi-slice (SMS) sequences.

A wide range of standard diagnostic sequences were used to test cardiac imaging using triggering with various settings of planes, phase encoding directions, Cartesian and radial k-space acquisition:

- Siemens single breath hold methods:
  - True FISP (Free Induction Decay Steady-State Precession),
  - True FISP - real time;
  - tirm_t2 (Turbo inversion recovery magnitude);
  - SPAIR (SPectral Attenuated Inversion Recovery);
  - PSIR (Phase sensitive Inversion recovery)
  - T2_haste (Half Fourier Single-shot turbo spin echo.

Individual parameters of used sequences are shown in Table 2. While the cardiac MRI was acquired using standard pulse sequence and typical parameters used in clinical practice, both standard (mprage, FLAIR etc.) and state of the art (multiband fMRI and DWI) pulse sequences were acquired with physiological data recordings for retrospective MRI data correction.

II. SYNCHRONIZATION OF CARDIAC AND RESPIRATORY ACTIVITY IN CMR

CMRI triggering and gating are the techniques necessary to provide high temporal and spatial resolution of the heart's image, which is constantly in motion, in real time [8], [29], [30]. Synchronization with a cardiac or respiratory cycle is performed. Besides the most prevalent technique for cardiac activity monitoring based on ECG [13], [31], other techniques are used in the clinical practice – such as vectorcardiograph (VCG) [32], [33] or a peripheral pulse (PPG, photoplethysmography) [34], [35]. In most cases, CMRI examination is used to trigger the MRI sequence during the relatively resting heart phase, which is the terminal phase of the diastole or the systole.

Synchronization respiratory activity is also used to ensure optimal heart image quality. At present, the most widespread method of reducing the artefacts caused by breathing is called breath hold method. However, when using this method, the scanning time decreases according to patient's ability to hold the breath, usually to about 20 seconds. One MR acquisition is acquired throughout a single breath hold, during this time, several heart cycles take place [5]. Nevertheless, in some patients with certain respirational diseases, this method cannot be applied. In these cases, real-time respiratory activity monitoring can be used for the synchronisation. The most commonly used probe for MRI respiratory triggering is the pneumatic respiration transducer located on the patient's chest [36].

Gating can be divided into two basic principles – prospective and retrospective. In the prospective gating or triggering, the MRI sequence is triggered only after the desired physiological phenomenon is detected (R wave of ECG, pulse wave peak, AO wave of SCG etc.). In the retrospective approach, the MR data is recorded continuously and grouped, after recording, according to the phases of the cardiac cycle [12], [13].

A. PROSPECTIVE TRIGGERING

In prospective triggering, the MRI acquisition is triggered by the R wave with a certain delay. Thus, the acquisition is consistent with the most mechanically resting phase of the cardiac cycle - the diastasis, which corresponds to the mean diastolic phase of the ECG signal. Prospective functional imaging depends on partial k-spatial acquisitions for a series of images that cover most of the cardiac cycle; the k-space is eventually filled by averaging the signals from the same cardiac phase during several heartbeats. This functional file starts with the R wave [29], [31], [37].

The interval is often set so that the detector deliberately ignores any high amplitudes to prevent false triggering by an ECG signal in any other way than by the R wave. However, this capability is problematic when sensing patients suffering from arrhythmia with ventricular extrasystole presence. In patients with premature heartbeats, the earlier R wave is omitted because the gradient impulses triggered by the

TABLE 2. Individual parameters of used MRI sequences.

	FOV Field of view (mm)	Resolution (pixel)	TE Time to echo (mm)	TR Time to repeat (mm)	TA Acquisition time (mm)	FA Flip angle deg	TI Inversion time	Slice thicknes (mm)
Trufisp - cine retrospective gating - heart	340×340	208×208	1.784	43.44	13.87	43	—	6 mm
T1 flash - heart	311×340	132×192	1.35	700	27 s	10	—	8 mm
Flash PSIR - heart	262×350	140×256	1.96	668	3.99	2; 20	TI = 100	—
T2 - MRCP sequence - T2 triggered - bile ducts	300×350	192×256	1.2 2.4	4	23 s	45	—	1.7 mm
T1 MPRAGE - brain	224×224	224×224	2.33	1770	3 min 37 s	8	TI = 900	1 mm × 240
T2 space - brain	224×224	224×224	147	2000	4 min 32 s	(auto)	—	1 mm × 160
T2 space Flair - brain	224×224	224×224	393	5000	5 min 52 s	(auto)	TI = 1800	1 mm × 160
EPI - DWI - brain	210×210	140×140	84.6	3700	10 min 5 s series 158 vols	78	bvals = 0,1500, 3000 0, 1500, 3000	1.5 mm × 92 MultiBand 8
EPI - Bold - brain	208×208	—	35.2	750	7 min 2 s series 550 vols	52	—	2 mm × 72 MutiBand 8
EPI - Bold - brain	134×134	64×64	16.6 35.6 54.5	600	10 min 18 s series 1000 vols	45	—	3.5 mm × 42 Multiband 6

previous R wave are still running. This process extends the acquisition, thereby extending the time necessary for holding the breath. Therefore, prospective gating is defenceless against R-R interval fluctuations not only throughout the examination, but also within one breath hold. When planning the acquisition window positioning for prospectively triggered examination, this cardiac variability must be considered. So as to capture another R wave, the acquisition window position should not be too close to the next R wave. The acquisition window, which is placed too close, can interfere with the next R wave and the corresponding R-R interval is then shorter. Knowing the patient's cardiac variability during the breath held is crucial; depending on the patient's physical condition, significant changes may occur. Therefore, a breath hold test is often required before the acquisition itself, when the appropriate cycle length is measured. During the examination, the operator must monitor changes in the cardiac cycle and appropriately adjust the prospectively triggered images [13].

B. RETROSPECTIVE SYNCHRONIZATION

Retrospective triggering allows continuous acquisition of MR data. Both the image and the ECG signal are scanned during several systoles and used to reconstruct the image by an appropriate grouping of the cardiac phase information. This procedure requires dynamic pulse sequences and an acquisition software decision. Retrospective gating uses complex methods for filtering interference. The main advantage of retrospective acquisition is the ability to collect data from all cardiac phases. The retrospective method, like prospective triggering, may have problems with arrhythmias and low R wave amplitudes. With heart rate variability or arrhythmia events, the systole and diastole periods are unevenly altered, and the retrospective software is unable compensate them with appropriate data segmentation into which errors are entered by improper triggering [13], [38]–[40].

C. ARTIFACTS

Artifacts during CMRI measurements may originate in both the patient and the measurement system. The blood flow in the heart can induce tension and create hydrodynamic artifacts. Since blood is an electrically conductive liquid whose movement produces an electric current added to the heart signal, a magnetohydrodynamic effect is produced. The electrical signal thus generated usually affects the T wave. If a T wave occurs at the time of rapid blood flow from the heart, the T wave is distorted. When synchronizing using VCG, which measures the spatial orientation of electrical activity in three dimensions, this effect can be suppressed because the cardiac electrical activity and the voltage generated by the magnetohydrodynamic effect arise in different planes and can thus be differentiated [9], [13].

Other problems such as abnormal heart conduction or unrelated physiological processes (e.g., muscle tremors) are additive to the above-mentioned noise. Optimal image quality requires an electrode placement that maximizes the R-wave peak while minimizing these basic artifacts. This can be achieved by placing the right hand and left foot leads in the central line of the chest. Extreme changes such as high amplitude system noise or small electrical currents caused by

a change in the magnetic field gradient are very worrying, but, due to the large difference in the frequency at which this noise and the sensed heart rate signal are found, high frequencies can be suppressed by filtering [13], [32].

Some scanners have the option of rejecting measurements at the time of anomalous rhythm and an acceptance window that allows R-R variability must be specified. This usually increases the acquisition time and a decision on a shorter scan time or better image quality must be made and the number of segments must be increased to reduce the acquisition time. Extreme deviations of the R-R interval should be overcome by prospective triggering instead of retrospective. Usually, a shorter R-R interval should be used for the acquisition window triggering. Its length must be slightly shorter than the shortest R-R interval measured in the ECG signal. The resulting CMR will represent an incomplete cardiac cycle, but it will be possible to calculate the ejection fraction.

To reduce distortion caused by the influence of the magnetic field, the electrodes and the associated connectors and cables should be made of non-ferromagnetic material. Continuous recording of the ECG signal and the triggering events is essential for early detection of problems. Interference may falsely trigger the scanner, thereby losing synchronization with the heart [13].

D. SENSING AT HIGH MR FIELD INTENSITY

In clinical practice, the use of magnet field intensity of 1.5 T or 3 T is currently widespread. MRI sensing at field intensity of 7 T promises to increase the signal-to-noise ratio (SNR) or noise suppression, to increase the contrast between the myocardium and the blood, to reduce the artifacts in the image, which leads to better temporal and spatial resolution. Therefore, monitoring of cardiac cycles is simpler and post-processing processes that are still time consuming are accelerated [41]. In comparison with sensing at 1.5, the contrast does not only increase in the short-time image of the heart perpendicular to the blood flow, but also in the long-term imaging of the heart, evenly with the blood flow. Hence, fine anatomical structures such as pericardium, mitral and tricuspid valves and associated papillary muscles are well identifiable. Due to the increase in SNR, it is possible to reduce the volume effects that may be useful for visualizing small, fast-moving structures [4], [42].

Reducing the noise level has a great advantage in MR angiography, where tiny vessels, such as coronary arteries, are better visible at an intensity of 7 T than at 1.5 T. In this context, time-resolved 3D flow display along with trace particle mapping is another interesting and rapidly developing area of high-intensity CMR. This approach promises new insights into the temporal and spatial evolution of blood flow in large vessels and in ventricles. The benefit of this enhancement would include improving morphological and functional evaluation of the normal or pathological cardiovascular system. In addition, the benefits of SNR in the area of capturing images at a high field intensity enhance the possibility of extending the current 4D phase contrast technique to whole heart acquisitions. The use of high field intensities can also be used in quantitative CMRI examinations for parametric mapping that allows non-invasive tissue assessment. For example, mapping at 7 T may simplify this operation by easier distinguishing of healthy tissues from myocardial regions with reduced perfusion [4].

III. CMRI TRIGGERING METHODS

In stronger magnetic fields, the ECG is significantly distorted by the artifacts. The VCG method is more resistant to these negative effects, however, even this method is inaccurate when ultra-high intensities of MR fields are used. When using intensities higher than 3 T, there is a problem with the increasing influence of the magnetohydrodynamic effect on the signal, making it more difficult to obtain a clear signal of sufficient quality for performing flawless triggering. While PPG measurements do not produce significant movement artifacts, the major disadvantage of PPG measurement is the delay between the cardiac activity and the output signal caused by the time needed for the blood pulse wave to spread from the heart to the sensing location, which is usually found on the peripheral parts of the body (most commonly the finger). This delay can be of several hundred milliseconds and depends on the patient's (patho)physiology [43].

As ultra-strong MRI fields become more widespread, the emphasis is being placed on addressing the rising ECG sensitivity to electromagnetic field interference and the magnetohydrodynamic effect, i.e. the need for better synchronization techniques is increasing [18], [43]. This leads to the development of the new methods of CMRI triggering, such as acoustic triggering, ultrasound triggering, or systems triggering directly from MR data, have begun to develop [18], [30], [44].

A. THE ACOUSTIC METHOD

Due to these pitfalls of ECG measurement during MRI acquisition, a stethoscope [18], [45]–[48] that senses a phonocardiographic (PCG) signal from which the first heart sound is determined as a triggering pulse has been designed. Unlike conventional ECG, heart sound sensing has several advantages – for example, it is easier to prepare the patient (the location of applying the sensor does not have to be shaved, the skin is not prepared by any chemical means, the sensor can be placed also over the clothes), the number of cables and sensors that need to be applied to the patient is reduced, or the induction of high voltages that may injure the patient is prevented [18], [49]. The ability of the PCG signal of both prospective and retrospective triggering, and, later, its effectiveness in clinical practice for ultra-high magnetic fields [43], [49], [50], has already been demonstrated on a field size of up to 3 T [18], [51].

The MRI acoustic control device consists of a sensor for sensing the PCG signal mounted on the patient's chest, wherein the signal conduction is provided by an acoustic waveguide [43] or optical fibre (in the case of conversion from acoustic to optical signal) [49], where no PCG device

interacts with a static magnetic, gradient, or radio frequency field. For optimal triggering, the following prerequisites should be met: 1. maximum latency of 35 ms between the R waves and the PCG triggering pulses, 2. signal without electromagnetic field interference, 3. resistance to the magnetohydrodynamic effect. The problem of acoustic signal measurement may be acoustic noise caused by gradient coil switching, which can be suppressed by measurement with another sensor and the subsequent signal processing [43]. It has been proved that, when triggered by the PCG signal, there are no motion artifacts or other visible disturbances or the hydrodynamic effect in all MR field measurements (in the range of 0.3 - 7 T). On the other hand, a significant increase in the T wave amplitude and other signal distortion are observed from the course of the VCG curve, where R wave detection demands considerable accuracy. Poor registration of the R wave then causes a reduction in myocardial/blood contrast and image sharpness [18], [43], [50]. It has been proved that motion artifacts occur only during ECG signal triggering when MR images are blurred due to erroneous R wave detection. The ECG heart rate error rate (especially at high amplitude or rapid signal rise locations, such as the initial oscillation forming the R wave) reaches up to 30 % [43], while, for PCG triggering, an error of less than 1 % is achieved at a field strength of 7 T [50]. A delay of about 30 ms between the detected R wave and the first sound that occurs during PCG measurement has no effect on CMR imaging using retrospective triggering, [18].

B. SELF GATING METHODS

To eliminate the need for extra hardware for CMRI synchronization, so-called self-gating techniques [29], [36], [52] are used. These techniques use motion information for triggering directly from MR signals, but at the expense of significant prolongation of the scanning time. The principle of the CMRI self-gating method consists in changes or movement of the volume in the image, where a series of consecutive echoes exhibit peak changes corresponding to proportional changes in the total transverse magnetization due to organ movement. This data is then processed and segmented to generate a signal replacing ECG, according to which the image is then reconstructed at each cardiac cycle. Most of these methods have already been successfully used for retrospective CMR triggering, which is not as sensitive to heart rate changes (as in prospective triggering) and provides image throughout the cardiac cycle, which is particularly important for the determination of diseased systolic or diastolic processes [29]. However, these techniques lag behind in the case of very high heart rate and some heart diseases, where myocardial contraction and relaxation are very mild throughout the cardiac cycle. Also, they are unsuitable for use in prospective triggering, which requires precise determination of the start-up delay, so that an acquisition window could be placed in the target phase of the cardiac cycle [18], [29], [39].

C. THE ULTRASOUND METHOD

An interesting alternative to standard ECG triggering is the use of an ultrasonic probe in Doppler mode. Ultrasonic recording allows RR intervals to be measured similarly as ECG, and, as for image quality, the method equals ECG and PPG. So far, this method of triggering has been verified on CMRI at an intensity of up to 3 T [8], [30], [53], [54], but it also promises usability at higher field intensities, due to the low susceptibility of the ultrasound signal to being influenced by the magnetic field, unlike the ECG signal, which is very often significantly distorted by the magnetohydrodynamic effect [55], [56].

D. THE OPTICAL METHOD

Some studies investigate the possibility of sensing cardiac activity by optical fibre, but only when used in rodents [46]. The sensor is orally introduced into the rat's oesophagus [46] or is placed on the chest to sense movement [57]. The advantage is the resistance of the optical fibre to the interference caused by the magnetic field; there are no movement artifacts in the image [58]–[61].

IV. DESCRIPTION OF THE MEASURING AND TRIGGERING SYSTEM HW AND SW

The SCG is a method for studying the mechanical vibrations which are produced by cardiovascular activity. Common sensors used for SCG monitoring are accelerometers. They can measure acceleration in three axis and give complete information about the heart movement.

The SCG, as monitoring technique, is receiving increasing attention. In special cases, such as monitoring CA during MRI, the accelerometer cannot be standardly used. The measured signal would be influenced by changing magnetic field and inducted currents.

In this paper, we proposed a SCG monitoring method that relies on non-magnetic materials which do not affect MRI examination. The ECG monitoring is standard monitoring technique for triggering of MRI by AO. To successfully develop the adequate system, we must firstly understand relations of ECG and SCG signal measured by proposed setup.

The presented equipment was different from the standard SCG monitoring tools and was therefore studied in detail. One of the most significant changes in standardized SCG measurement is that our system measures the acceleration in one vector perpendicular to the location of the sensor on the patient's chest. Sensing of the patient's SCG signal is conducted by means of a plastic funnel (produced by the 3D printing method), which is fixed to the patient's chest by means of an elastic textile belt in the area where the heart is located. A PVC acoustic tube is attached to the end of the funnel, and this tube is brought into the control room, where it is subsequently connected to a measuring microphone. In this way, a closed acoustic environment is created which is highly resistant to external vibrations and sounds. The source of the signal is the movement of the patient's skin

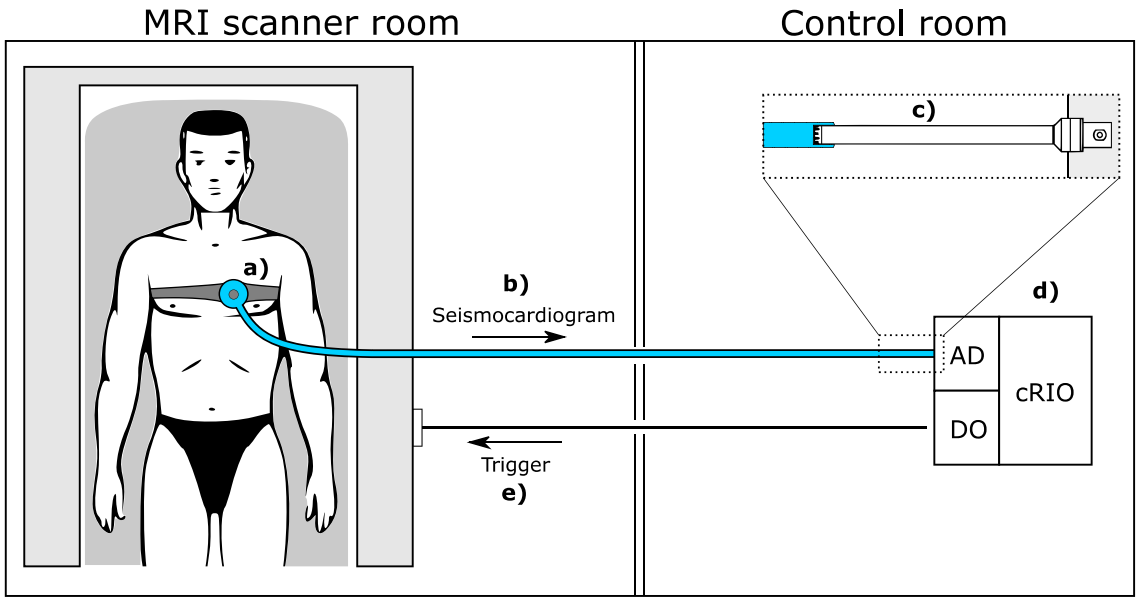

FIGURE 3. The schematic diagram of the measuring and triggering system; a) Plastic funnel fixed by elastic belt at patient chest, b) Acoustic tube for transmitting modulated pressure by the patient's heart, c) Measuring microphone, d) Analog input, computing unit and digital output, e) Triggering signal for magnetic resonance imagining.

below the sensor. The patient's skin forms a membrane that moves due to the expulsion of blood from the heart to the aorta and the pulmonary veins. This movement may include superimposed interference caused by uneven skin movements due to heterogeneous chest structure. As a result, the shape of the SCG curve is directly dependent on the location of the sensor on the chest. The patient's skin movement vibrates the particles of the acoustically closed environment inside the funnel and the resulting pressure oscillations spread through the tube to the measuring microphone which converts them into a voltage signal. The microphone output is brought into the input of the analogue-to-digital converter (ADC), where it is digitized and then processed and analysed in the control unit. Based on the signal analysis performed, the control unit generates a triggering signal for prospective and retrospective gating of magnetic resonance. The schematic diagram of the described system is shown in the following Fig 3. The most important advantage of this system is its resistance to electromagnetic and acoustic interference in magnetic resonance, and its ability to measure during imaging.

The basic advantage of this configuration of the measuring device is the fact that the SCG signal transmitted is not largely modified when passing through the acoustic conduction. Measurements that were conducted using different acoustic conduction lengths (0 to 30 m) revealed that only minor nuances in the area of the frequencies characteristic of the SCG signal (i.e. 0 to 30 Hz) occur. The difference observed in the spectrum of the signal measured at the beginning and at the end of the acoustic conduction is up to $\pm$ 5 dB (it differs by signal deviation). An important parameter is the difference seen in the temporal domain of the signal in the form of signal delay. This is due to the limited maximum velocity of the excitation transfer depending on the media material inside the acoustic conduction, i.e. air. The distance-velocity lag is variable and directly related to the length of the acoustic conduction and the propagation of the pressure wave outside it. In this particular case, the acoustic conduction had a length of 11 m; according to the measurement, the distance-velocity lag of the signal measured was about 37.5 ms (i.e. the propagation rate is 290 ms^{-1}). Knowing the value of the distance-velocity lag is necessary for the correct setting of the time delay from the R-oscillation detected. When the SCG signal delay time correction is performed properly, the operator can access imaging when tuning the time delay as well as when using the ECG signal. Magnetic resonance measurements also revealed that the interference signals produced during the scanning sequences (vibration of the magnetic resonance structure and its acoustic manifestations) have a typical distance of about 20 dB from the useful signal.

The measuring and triggering systems were completely designed on the basis of virtual instrumentation. cRIO-9073 platform [62] made by National Instruments was used as the control unit [63], [64]. The cRIO platform was selected as it consists of a combination of a gate array (FPGA) and a controller with VxWorks real-time operating system (RTOS). This interconnection enables fast analysis of the signal measured and very accurate generation of the triggering signal over time with a resolution ranging from microseconds to hundreds of nanoseconds. The Human Machine Interface (HMI) is not part of the selected cRIO model, so a PC, which is connected to the cRIO via an Ethernet interface, is also included in the control unit. The SCG signal is sensed using a GRAS 40PP microphone [65]–[67] with a frequency range from 10 Hz to 20 kHz and a sensitivity of 50 mW/Pa. The cRIO used has four slots for connecting input/output modules. For microphone signal measurement,

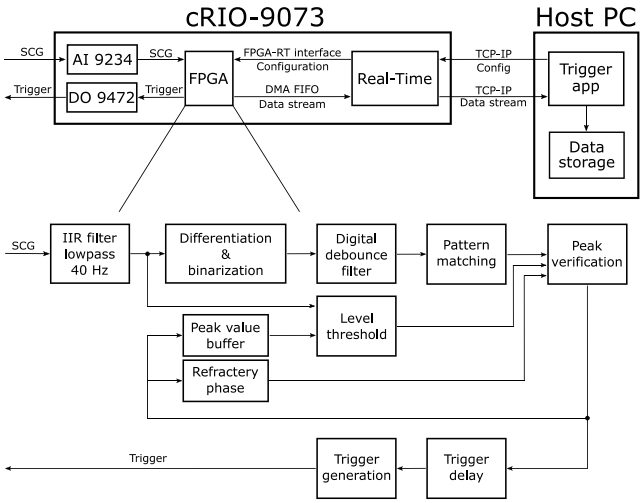

FIGURE 4. **A detailed description of the control unit with a detailed description of the gate array logic.**

the cRIO-9250 module [68] was selected, which features 2 simultaneous ADC channels with a 24-bit resolution, a $\pm$ 5 V input range, and a sampling rate of up to 102.4 kS/s. The module is used for very accurate vibration measurement using microphones and accelerometers. The triggering signal is generated using the second cRIO-9472 module [69], which consists of 8 digital outputs, 6 V - 30 V compatible, capable of delivering a current of up to 0.75 A per output channel.

A detailed diagram of the entire control unit with a detailed analysis of the lowest gate array layer is shown in the following Fig. 4. The measuring and triggering system function is controlled by a three-layer SW application created in the LabVIEW [70]–[72] development environment and its expansion modules (Real-Time and FPGA). The lowest and most important SW layer is implemented for FPGA. Its task is to read values from ADC, process and analyze the digitized signal in real-time and, subsequently, generate a digital triggering signal of a user-defined width and an adjustable delay. The processing involves digital signal filtering with a fourth-order low-pass infinite impulse response (IIR) filter with Butterworth approximation and a cut-off frequency of 40 Hz. We used IIR filter implementation because it generally requires less FPGA resources (especially memory elements) than finite impulse response (FIR) filter implementation. Additionally, the FIR filter may cause longer time delay, which is highly undesirable. We tested both FIR and IIR filters in LabVIEW development environment before we implemented it using the FPGA module. Both filters performed nearly the same. The nonlinearity of the IIR filter phase frequency response had no effect on the SCG signal morphology. For selected sampling frequency, the FIR filter implementation would require around 400 taps to achieve the same amplitude frequency response as IIR filter. That would cause slightly longer (a few milliseconds) time delay of the processed SCG signal leading to a delay in generating the triggering signal. The filtered signal is analyzed by a simple peak detector implemented directly into the FPGA logic. The user can configure the detector by defining the refractory time (time after the detected peak when the system does not expect a new peak to occur) and the signal level threshold coefficient. The implemented gate array logic also allows transmitting the measured signal waveform, the trigger generated, and the information on the peak detected to the RTOS microcontroller via the DMA FIFO channel. The microcontroller then forwards the signals to the PC, where they are displayed to the user/operator, via the Ethernet interface.

The middle layer of the SW application is implemented for the RTOS controller and serves as a bridge for data transfer between the FPGA and the user PC. Two TCP servers are implemented here, wherein the first server receives configuration commands from the user PC, recalculates the values, and then writes them to the registers shared with the gate array. The second server reads the data stream from the DMA FIFO gate array and sends it to the connected user PC. The highest SW layer is implemented on the PC and includes two TCP clients that connect to servers running on the RTOS and a user interface allowing the configuration of the cRIO system and displaying the waveform of the signal measured, the peak detected and trigger generated. The below-listed Fig. 5 shows

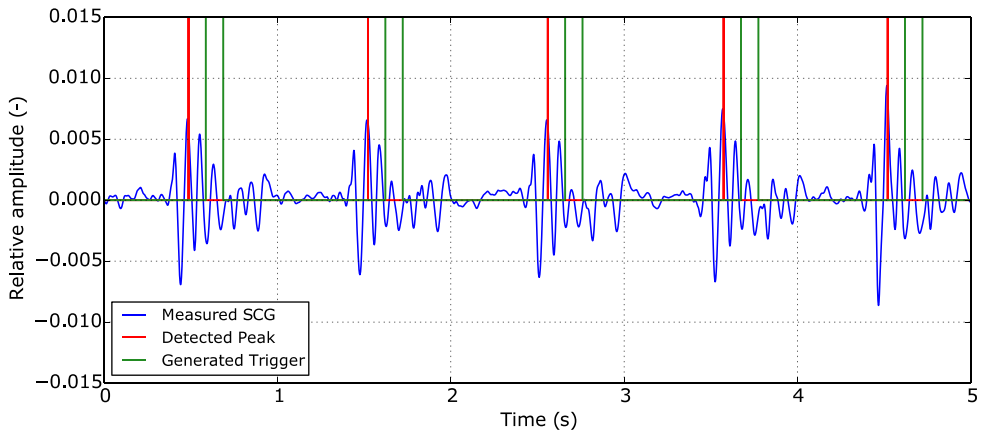

FIGURE 5. **The waveform measured and the signals generated by the gate array logic (SCG signal with detected peaks generated trigger).**

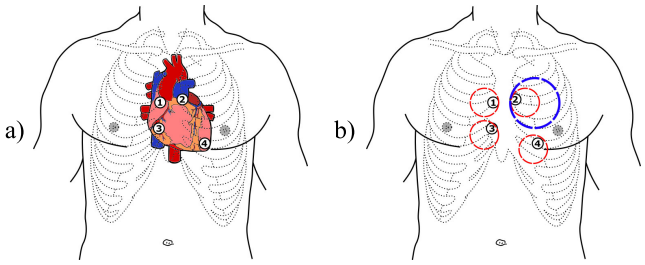

FIGURE 6. The illustration of the sensor placement. a) Measurement sites of mechano-acoustic signals with respect to the heart anatomy: 1. Aortic, 2. Pulmonary, 3. Tricuspid, 4. Bicuspid; b) Recommended areas for the placement of the sensors for the heart sounds measurement (red) and the seismocardiography (blue).

FIGURE 7. Placement of the sensor tested on the patient's body.

a graph containing all the signals measured and generated by the gate array logic.

Fig. 6 shows the illustration of probe positioning with respect to the areas used for heart sounds auscultation. The optimal location of the seismocardiograph sensor [73]–[76] was selected as an area with audible heart sounds and a surface ensuring the hermetic sealing of the measurement system.

Fig. 7 shows the placement of the SCG sensor tested on the patient's body. The sensor is fixed by means of an elastic belt, where you can the acoustic conduction emerging from the belt. A commercial ECG system can also be seen in the figure.

V. EXPERIMENTS

For triggering and physiological signals acquisition with Siemens Physiological Measurement Unit (PMU) using sensor – ECG electrodes, respiratory cushion and pulse sensor - directly at the patient via the PERU (ECG, respiration) and PPU (pulse). [MR System | Operator Manual Print No. M7-04001.621.04.01.24] The Siemens device physiological data export is complicated and, moreover, the sampling rate is relatively low, so BRAINVISION - BrainAmp ExG system [77] made by BRAIN Product is used for recording the signals for the purpose of retrospective correction and removal of the physiological effects from

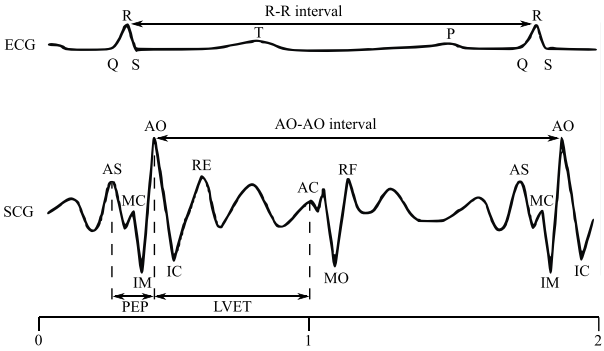

FIGURE 8. A typical resting seismocardiogram (SCG) and matching electrocardiogram (ECG).

the MR data. The curves presented below come from the BRAINVISION system. For the purposes of this article, all three devices, PMU, BrainAmp ExG and SCG, were usually used simultaneously.

Standard anatomical (T1 mprage, T2_spc_T2_spc_FLAIR), fmri (epi_bold) and diffusion sequences, as well as state-of-the-art research pulse sequences (mp2rage, and diffusion and functional imaging sequences using parallel layer excitation - SMS or also called multiband), were used for testing SCG and respiratory. These sequences are then the most demanding in terms of high-frequency interference, magnetic and acoustic interference and vibration caused by the gradient system when the noise of these methods can exceed 120dB.

A. ECG VS. SCG WAVEFORMS AT SELECTED SEQUENCES

To demonstrate the functionality of the SCG system tested from the point of view of vital signs monitoring during the selected sequences, short time domain previews, a) ECG signal and b) SCG signal, are interpreted below. The authors divided these previews into three groups:

1) both the ECG and SCG commercial systems work well, see Fig. 10 and Fig. 11;
2) the SCG system tested works well, the commercial ECG system introduces errors (undetected or falsely detected R) into the measurement, see Fig. 12, Fig. 13 and Fig. 14;
3) the SCG system tested works well, the commercial ECG system does not work at all, see Fig. 15 and Fig. 16.

The criterion of functionality is defined by the heart rate in the case of the ECG signal, namely, it is based on the detection of the R-R interval and, in the case of the SCG signal, it is based on the detection of the AO-AO interval, see Fig. 8.

Fig. 9 further shows the delay (approximately 45 - 120 ms) of AO after R; this is caused by biological processes in the human body, but also by the measuring system itself (about 50 ms), where the signal propagation time of the transmission medium must be taken into consideration (approx. 3.4 ms per meter) as well as the delay caused by signal processing (filtration) (approximately 15 ms).

Fig. 10 shows a preview of a) ECG and b) SCG before running the sequence (resting state) [78]–[80]. Obviously,

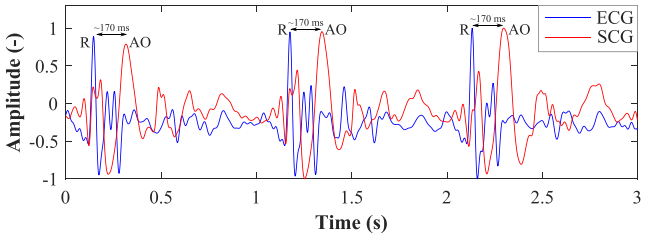

FIGURE 9. The delay (~170 ms) between significant points (R-AO) detected in ECG and SCG on measured subject.

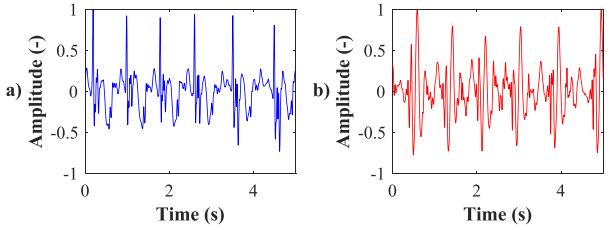

FIGURE 10. A waveform of a) ECG and b) SCG before running the sequences (Resting state).

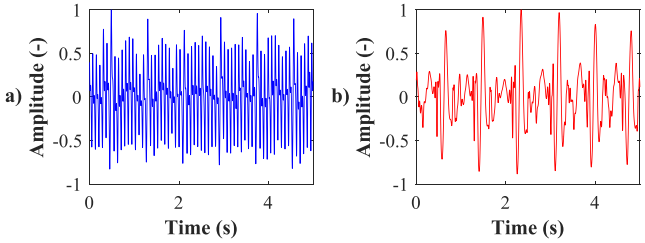

FIGURE 11. A waveform of a) ECG and b) SCG during the sequence (T2 weighted with fat suppression using the SPAIRE method).

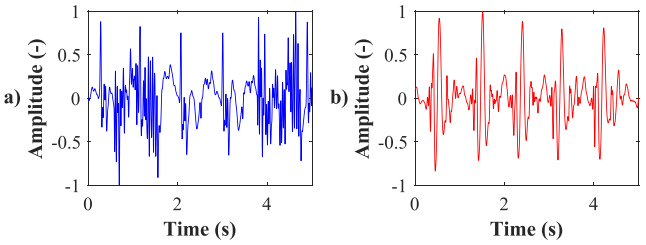

FIGURE 12. A waveform of a) ECG and b) SCG during the sequence (TRUE FISP sequence used).

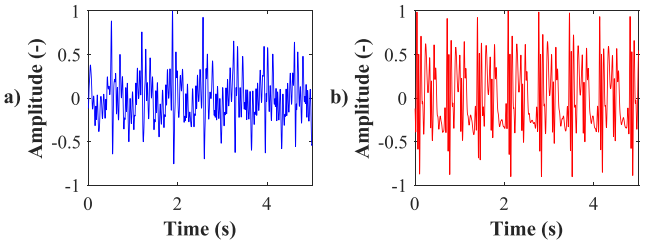

FIGURE 13. A waveform of a) ECG and b) SCG during the sequence (T1 weighted with PSIR saturated myocardial signal suppression).

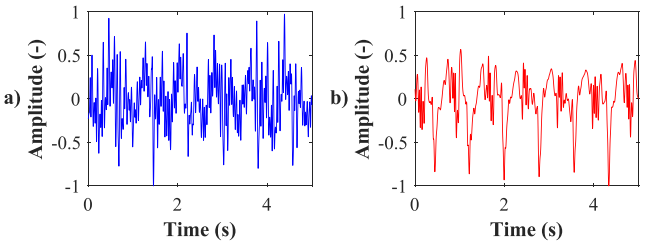

FIGURE 14. A waveform of a) ECG and b) SCG during the fMRI BOLD sequence.

the signals measured are of good quality, without artifacts and interference, so there is no problem in detecting the R-R and AO-AO intervals the detection of which is absolutely necessary for cardiac triggering based on the cardiac activity.

Fig. 11 shows the waveforms of a) ECG and b) SCG with the sequence already running (T2 weighted with fat suppression using the SPAIRE method). Obviously, the sequence had no effect on the SCG signal, whereas the ECG signal is greatly degraded by switching of the high frequency pulses during the running sequence. However, the ECG signal is still useful for determining R-R intervals.

When looking at Fig. 12, Fig. 13, it is obvious that the ECG system will cause a significant error in cardiac triggering because we are unable to accurately detect the R-R interval. The TRUE FISP sequence used to make a kinetic study, or T1 weighted with PSIR saturated myocardial signal suppression. There is no problem with the detection of the AO-AO interval in the SCG system, i.e. cardiac triggering is possible. In Fig. 12 and Fig. 13, the ECG system may detects false R intervals (e.g., between the 4th and 5th second, Fig. 12a), resulting in inaccurate sequence triggering, which may cause artifacts in the image.

Fig. 14 shows that, with the ECG signal, we are not able to correctly detect the R-R interval (there is a large number of undetected and falsely detected R oscillations), whereas, with the SCG signal, there is no problem with the AO-AO interval detection. The sequence used was fMRI BOLD.

When looking at Fig. 15, Fig. 16, it is obvious that, with the ECG system, we are not able to detect R oscillations at all, since the signal is completely jammed by high-frequency interference, which was, due to aliasing, mirrored into the frequency domain of the useful ECG signal and cannot be filtered. The SCG system tested works smoothly again. Fig. 14 is a sequence of diffusion weighted echo using epitechnics which is characterized by a high potential for triggering involuntary nerve or muscle spasms. Fig. 15 is a sequence of 3D T2 weighted TSE ECHO - SPACE.

B. INFLUENCE OF SUBJECT MOTIONS IN POSTURAL POSITION ON SCG SIGNAL

As part of our research we did an assessment of the influence of subject motions in postural position on quality of acquired SCG signal. For this experiment we selected one male subject and measured the SCG signal while the subject was performing motions typical for postural position, which subject

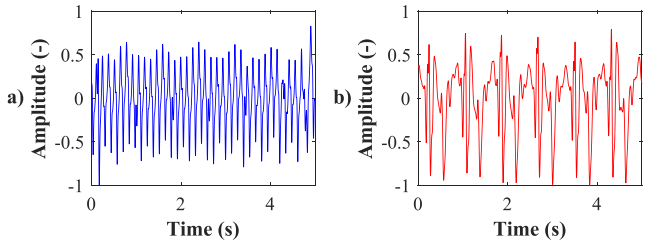

FIGURE 15. A waveform of a) ECG and b) SCG during the sequence of the diffusion weighted echo using epitechnics.

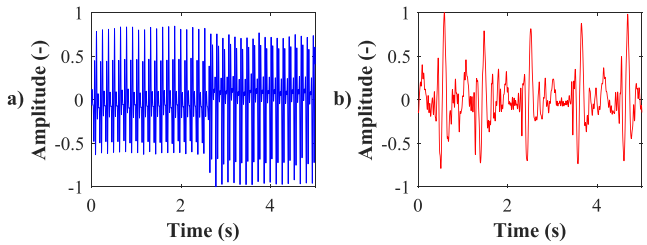

FIGURE 16. A waveform of a) ECG and b) SCG during the sequence of the 3D T2 weighted TSE ECHO - SPACE.

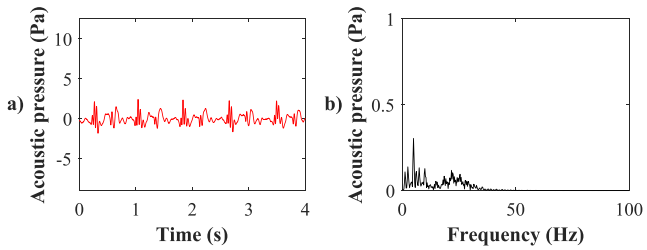

FIGURE 17. Example of: a) measured SCG signal when subject lies still and b) its corresponding amplitude frequency characteristics.

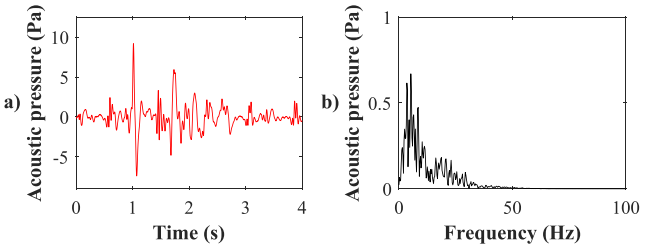

FIGURE 18. Example of: a) measured SCG signal while subject was speaking and b) its corresponding amplitude frequency characteristics.

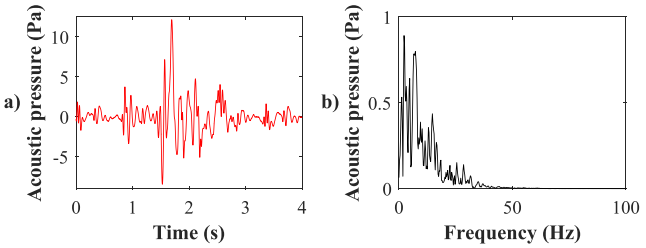

FIGURE 19. Example of: a) measured SCG signal while subject performed torso twitching motions and b) its corresponding amplitude frequency characteristics.

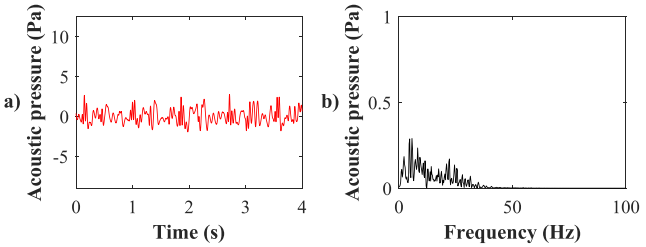

FIGURE 20. Example of: a) measured SCG signal while subject performed torso wriggling motions and b) its corresponding amplitude frequency characteristics.

occupies during MRI exam procedure. Performed motions were:

- head motions (slow turning to sides and slight leaning forward and backward),
- restless leg motions (twitching, slight turning and bending),
- speaking,
- heavy and deep breathing,
- torso wriggling (slight motions to sides),
- torso twitching (trying to get thorax and head up for repositioning).

Acquired SCG signal was only processed by the lowpass filter with configuration described in the previous section. In case of head motions, leg motions, slight torso wriggling and heavy or deep breathing, there were only minor distortions of the SCG signal. These motions only had a slight impact on the performance of peak detection algorithm. Speaking and torso twitching was causing considerable distortions of the signal, that made the correct detection of AO peak impossible. Frequency components of analyzed motion artefacts occupy the same band as components of SCG signal (1 Hz - 40 Hz). This makes filtration of distorted SCG signal using conventional linear IIR or FIR filters impossible so advanced signal processing methods would have to be employed. Fig. 17 to 20 display samples of SCG signals in time and frequency domain acquired when patient lays still and when performing selected motions. To illustrate the influence of motion artefacts in comparison with reference signal (patient lies still, Fig. 17), we deliberately used fixed ranges for Y-axis in these figures. In conclusion, motion artefacts can cause problems with peak detection and thus could devaluate the results of MRI exam due to incorrect triggering. However these motion artifacts would propagate into acquired MR exam images even if the triggering was accurate and devaluate the MRI exam results anyway. For this reason the patient is required to lie as still as possible during the MRI exam which, in case of cardiac monitoring lasts only about 10 to 15 seconds.

It is clear that the morphology of the individual SCG curves changes, see Fig. 11b) to Fig. 16b). This is due to the different locations (more in the following paragraph), the size of the contact area between the patient's body and the sensor, but also the pressure of the measuring sensor, and, moreover, the waveforms from different subjects (men vs. women), various BMIs, etc.

Two volunteers, a man and a woman, participated in a sensor placement experiment. According to the measurement (Fig. 21), the shape of the SCG signal is directly dependent on the sensor location (Fig. 6). Although the signal does not

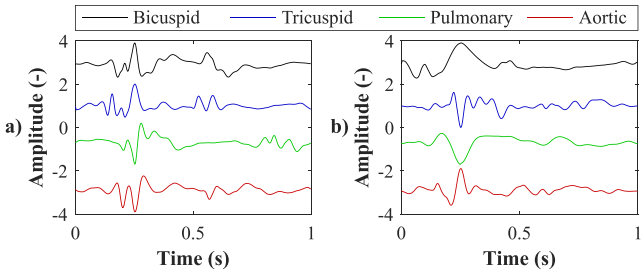

FIGURE 21. Representation of averaged and normalized SCG signal from a) Male and b) Female patient.

match the typical SCG curve, it always contains a significant peak that could be used to detect the heart cycle. To map this phenomenon, an additional study outside the MRI would have to be performed to map the characteristic curve shape depending on the sensor position. Furthermore, this information could be incorporated into the heart cycle detector to increase its accuracy.

C. RESULTS

In our experiments, we considered the ECG as the ''gold standard'' since the ECG-based systems are the most commonly used in clinical practice. According to the professional public, they reach the highest accuracy from the perspective of cardiac triggering. However, this argument is not sufficient to call the ECG system ''gold standard''. All ECG signals, which were used for the evaluation, were classified semi-automatically in the R-R intervals determination. This way, we gained the total number and time position of the heart beats in individual subjects (e.g. 821 beats in subject_1, etc.). Also, we took into account the time delay between ECG and SCG signal during analysis so that the distortion could not occur. Thus, we could establish our annotations for the verification of the SCG system.

For the relevant verification, only the sections where the reference ECG was recorded for us in good quality (i.e., the R-oscillations could be demonstrably detected) were deliberately selected, see Fig. 8. The data were obtained from 18 different patients (10 men and 8 women aged 20 to 45, all healthy, all with ethics committee approval). It should be noted that the SCG system tested is completely immune to electromagnetic and acoustic interference during all the sequences tested. Thus, it can be said that it achieves better results than the ECG reference, which is strongly influenced by the nature of the interference during the running sequence.

Fig. 22 includes a comparison of ECG and SCG signals along with the detection of significant points in these curves. A significant point (AO) in the SCG signal monitored should be detected within a range of $\pm$ 50 ms from the R wave detected in the ECG signal. Fig. 22a) shows a section where accurate detection of a significant SCG signal point was achieved in accordance with the reference ECG signal. Therefore, these points were labelled as true positive (TP). On the contrary, Fig. 22b) shows a signal section where there is an error in detecting a significant SCG signal point. If a point was detected outside the defined interval, it was labelled false positive (FP). On the other hand, false negative (FN) detection occurred when, in the range of $\pm$ 50 ms from the R wave detected, AO wave detection did not occur in the SCG signal. These errors appeared in sections where MO wave reaches a magnitude comparable to AO wave, so it was detected as an FP peak. Consequent AO wave was therefore not detected, as the detector refractory time, when the system is inactive, was still running because it does not expect a new peak to occur.

It is also important to note that the points shown in Fig. 22 are located in some places outside the peak of the ECG signal peak. This is due to the fact that the DC component was removed during the signal analysis, and, subsequently, detection in this signal was conducted. Thus, in the resulting signal, the detected points manifest themselves in the correct period of time, but at a different voltage level.

For all 18 patients a detection of significant points in reference ECG and tested SCG signals (samples shown in Fig. 23 to 30) was performed and based on the analysis described in Fig. 22, their binary classification (a decision whether the significant point falls into the category of TP, FP or FN) was conducted. Results of binary classification were then used to determine 4 performance parameters of peak detection in SCG signal. First parameter is sensitivity (SE, true positive rate or recall, see equation (1)), it measures the percentage of correctly identified peaks. Next Positive predictive value (PPV or precision, see equation (2)) measures percentage of identified peaks that are truly correctly identified as positive. Further Accuracy (ACC or statistical bias, see equation (3)) defines ration of correct identification to all identifications made. Finally F1 score (see equation (4)) considers both SE and PPV as a harmonic mean of these two parameters. In medical tests, results above 95 %, mean high creditability of tested method or system [58], [81].

$$ACC = \frac{TP}{TP + FP + FN} \cdot 100\ (\%). \tag{1}$$

$$SE = \frac{TP}{TP + FN} \cdot 100\ (\%). \tag{2}$$

$$PPV = \frac{TP}{TP + FP} \cdot 100\ (\%). \tag{3}$$

$$F1 = 2 \cdot \frac{SE \cdot PPV}{SE + PPV}\ (\%). \tag{4}$$

In the medical field, the Bland-Altman (mean-difference) plot is used to compare the results of two independent measurements of the same variable. The principle of this method is based on determination of the differences between individual results of two measurements, see equation (5), where X and Y are vectors of results of the individual measurements. Difference vector is then used to determine mean value μ and 1.96 multiple of standard deviation 1.96σ of all differences. Next vector of mean values of individual results of the two measurements, see equation (6), is determined. Finally the Bland-Altman plot is constructed using the vector of mean values (X-axis) and vector of differences (Y-axis). Also a

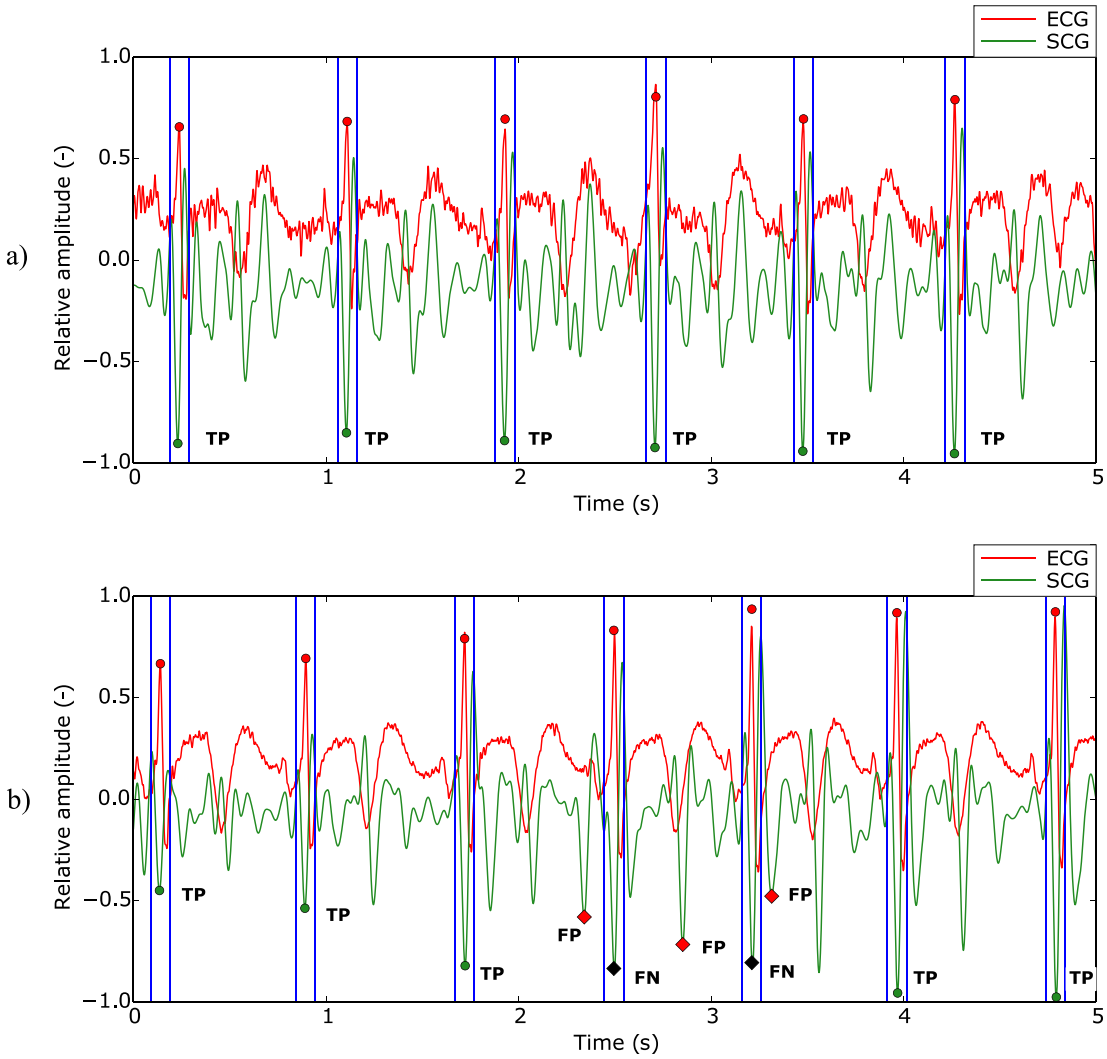

FIGURE 22. Evaluation of detection of significant points in ECG (Red) and SCG (Green) signals: A) successful detection section - significant points were detected in the SCG signal within an interval of ± 50 ms (blue) from the detected R wave in the ECG signal, thus labelled as true positive (TP); B) an example of a false positive (FP) and false negative (FN) detection section, the points were detected outside a given interval or were not detected in the given interval.

bold horizontal reference line is drawn at μ, this line represents mean difference between all measurements and if it significantly differs from 0 then it indicates fixed bias in the measurement. Additional two horizontal lines, known as limits of agreement, are drawn at $\mu \pm 1.96\sigma$, they represent range of agreement, within which the differences between the two measurements are expected to fall with 95 % probability (assuming the data comes from normal distribution) [58], [81], [82].

$$\overrightarrow{D} = (D_1, D_2, \ldots, D_n), \quad \text{where } D_i = X_i - Y_i. \tag{5}$$

$$\overrightarrow{M} = (M_1, M_2, \ldots, M_n) \quad \text{, where } M_i = \frac{X_i + Y_i}{2}. \tag{6}$$

The below-listed figures (Fig. 23 to 30) show a) a preview of the reference ECG signal section during the examination, b) a preview of the SCG signal section tested. The last subfigure c) represents the Blant-Altman graph, which statistically assesses the determination of vital signs during the examination, where the length of the determined R-R interval was used as a reference and as the evaluated length of the determined AO-AO interval. These waveforms are displayed for selected subjects tested; the length of the examinations during each sequence, but also during the resting state, was different.

Table 3 summarizes the achieved results of Bland-Altman analysis (columns μ and 1.96σ) and binary classification in all 18 subjects with those displayed in Fig. 23 to 30 being highlighted in bright green and bright red colors. Bland-Altman analysis indicates a difference bias for subject 1, 2, 3 and 5 with subject 1 having the worst result of -0.63 bpm. Also limits of agreements for these subject are significant, ranging from 6 bpm to 10 bpm. This results correspond with results of binary classification, which shows higher number of false positives (FP) and false negatives (FN) for mentioned subjects and also ACC and F1 parameters are lower in comparison with other subjects. These worse results are

TABLE 3. Summarization of the results achieved on all subjects tested.

Name	N (-)	TP (-)	FP (-)	FN (-)	μ (bpm)	1.96σ (bpm)	ACC (%)	SE (%)	PPV (%)	F1 (%)
subject_1	821	762	31	28	-0.630	10.16	92.81	96.45	96.09	96.27
subject_2	1110	1081	11	8	-0.340	7.13	98.27	99.26	98.99	99.12
subject_3	914	888	14	12	-0.330	8.38	97.15	98.66	98.44	98.55
subject_4	1003	998	3	2	-0.020	1.10	99.50	99.80	99.70	99.75
subject_5	899	879	11	9	-0.280	6.01	97.77	98.98	98.76	98.87
subject_6	831	829	2	1	-0.010	0.59	99.63	99.75	99.87	99.81
subject_7	887	885	1	1	-0.010	0.84	99.77	99.88	99.88	99.88
subject_8	721	719	1	1	-0.010	1.37	99.72	99.86	99.86	99.86
subject_9	731	729	1	1	-0.020	1.47	99.72	99.86	99.86	99.86
subject_10	603	601	1	1	0.020	0.89	99.60	99.83	99.83	99.83
subject_11	577	573	2	2	-0.003	1.82	99.30	99.65	99.65	99.65
subject_12	573	567	3	3	-0.003	1.70	98.95	99.47	99.47	99.47
subject_13	754	746	4	4	-0.030	3.51	98.96	99.47	99.47	99.47
subject_14	831	822	4	5	-0.030	3.55	98.91	99.39	99.51	99.45
subjekt_15	976	959	9	8	0.035	3.17	98.25	99.17	99.07	99.12
subjekt_16	1034	1020	6	8	-0.012	1.91	98.64	99.22	99.41	99.31
subjekt_17	1001	992	5	4	-0.017	1.26	99.10	99.59	99.49	99.54
subjekt_18	922	907	7	7	-0.026	2.12	98.47	99.23	99.23	99.23
Total	**15178**	**14956**	**116**	**106**	**-**	**-**	**98.53**	**99.29**	**99.23**	**99.26**

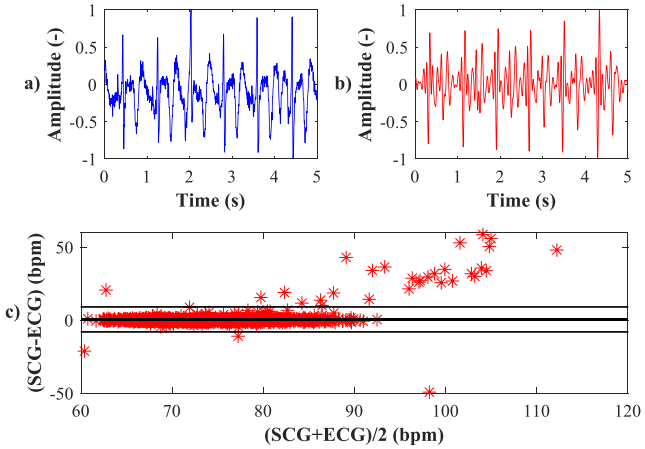

FIGURE 23. Statistical analysis. a) ECG (R-R), b) SCG (AO-AO) and c) Bland-Altman plot for subject_1.

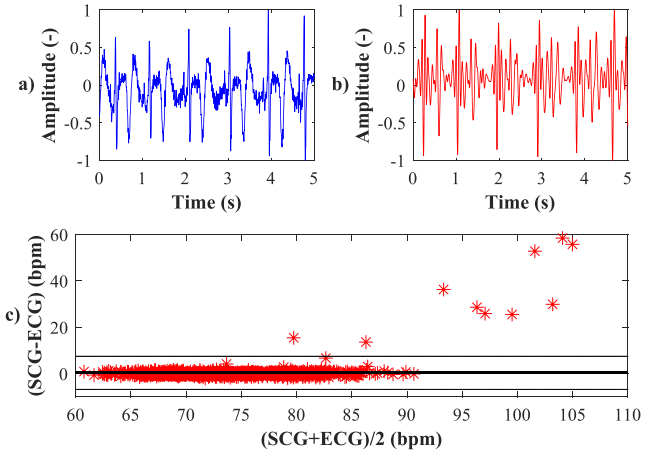

FIGURE 24. Statistical analysis. a) ECG (R-R), b) SCG (AO-AO) and c) Bland-Altman plot for subject_2.

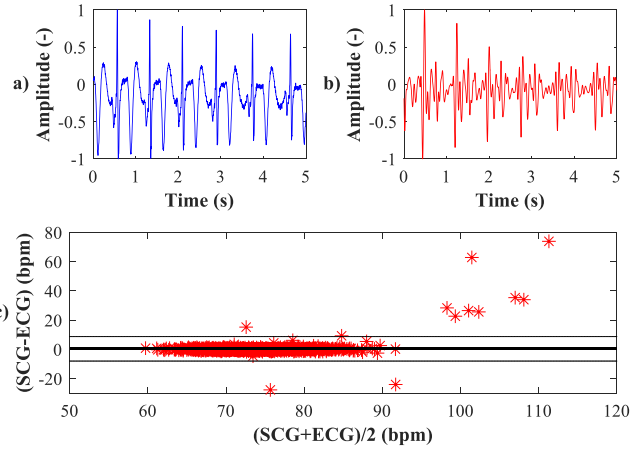

FIGURE 25. Statistical analysis. a) ECG (R-R), b) SCG (AO-AO) and c) Bland-Altman plot for subject_3.

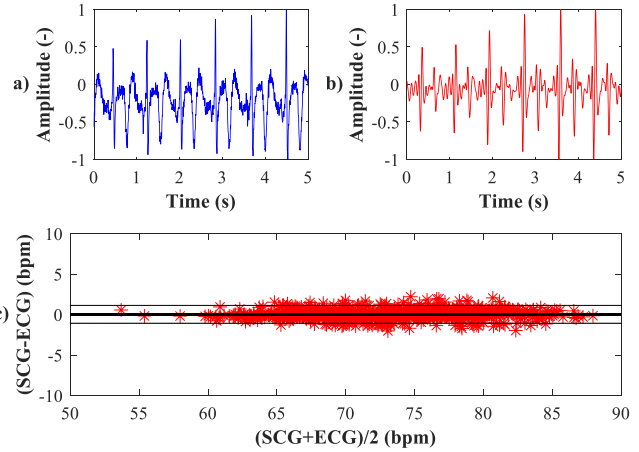

FIGURE 26. Statistical analysis. a) ECG (R-R), b) SCG (AO-AO) and c) Bland-Altman plot for subject_4.

mainly caused by presence of outliers in determined heart rates as shown in Fig. 23, 24, 25 and 27. Outliers are results of either movement artefact or imperfect sensor positioning. Both issues could be solved by employment of more

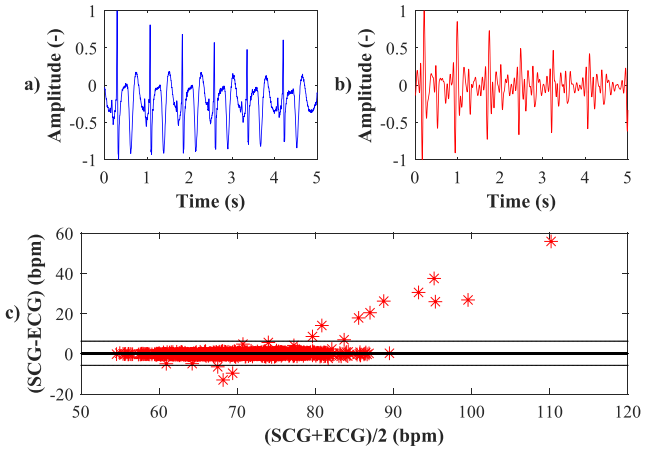

FIGURE 27. Statistical analysis. a) ECG (R-R), b) SCG (AO-AO) and c) Bland-Altman plot for subject_5.

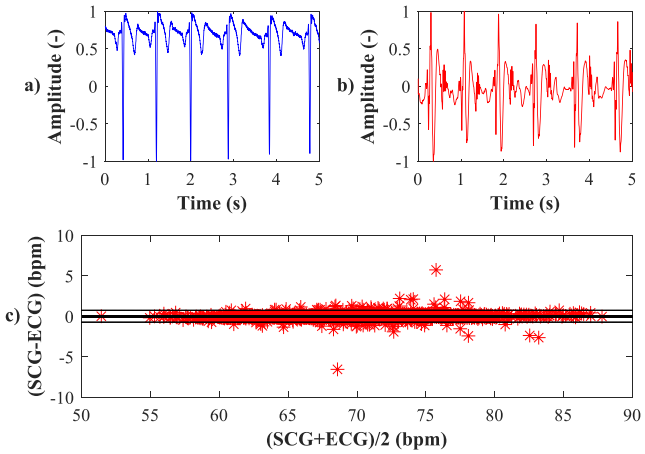

FIGURE 28. Statistical analysis. a) ECG (R-R), b) SCG (AO-AO) and c) Bland-Altman plot for subject_6.

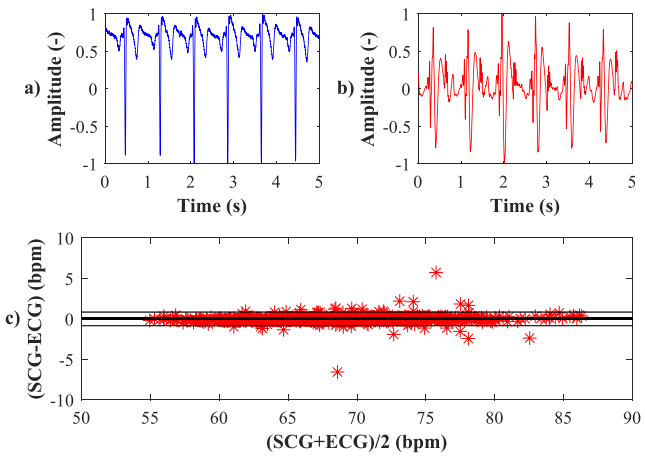

FIGURE 29. Statistical analysis. a) ECG (R-R), b) SCG (AO-AO) and c) Bland-Altman plot for subject_7.

advanced signal preprocessing of SCG signal and by increasing robustness of peak detection algorithm, which could be subject of further system improvements. Sensor repositioning is not an option, because it would significantly prolong patient preparation phase, which is highly undesirable in

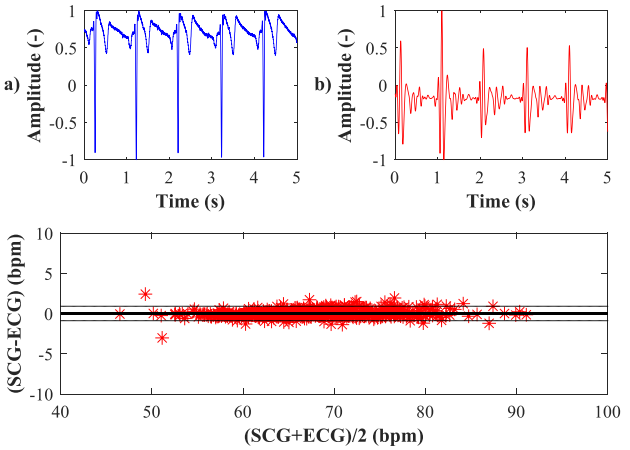

FIGURE 30. Statistical analysis. a) ECG (R-R), b) SCG (AO-AO) and c) Bland-Altman plot for subject_10.

clinical practice. Best results were achieved for subjects 4, 6, 7 and 10 (Fig. 26, 28, 29 and 30) with difference bias to be almost zero (-0.02 for subject 4) and limits of agreement in range from 0.59 bpm and 1.1 bpm. Binary classification results shows both ACC and F1 parameters to be over 99.7 %, which indicates almost perfect match. Results from remaining 10 patients have almost zero difference bias, considerably low limits of agreements in range from 1.37 bpm to 3.55 bpm and their ACC and F1 parameters lies in range of 98.9 % to 99.7 %. Last row of the Table 3 shows results of binary classification of detected peaks obtained from all measured subjects altogether. In total, 15 719 heart beats (peaks) were detected, with 14 956 correctly identified as true positive peaks, 116 incorrectly detected false positive peaks, and 106 missed peaks (false negative). For all subjects the total accuracy reached 98.53 % and F1 score reached 99.26 %. The results prove that the SCG signal can be used as substitute for ECG signal during magnetic resonance exam with reliability of correct heart beat detection reaching up to 99 %.

In the case of this work, ECG is used as the reference method, and SCG is used as the test method. The results of the ACC, SE, PPV and F1 parameters are marked as accurate if they exceed 95 % [58], [81].

D. CARDIAC TRIGG ECG VS. SCG

A wide range of standard diagnostic sequences was used for cardiac imaging using triggering. Siemens single breath hold methods True FISP (Free Induction Decay Steady-State Precession), True FISP – real time; tirm_t2 (Turbo inversion recovery magnitude); SPAIR (SPectral Attenuated Inversion Recovery); PSIR (Phase sensitive Inversion recovery) and T2_haste (Half Fourier Single-shot turbo spin echo) with various settings of planes, phase encoding directions, cartesian and radial k-space acquisition, using all previously mentioned methods of cardiac triggering SCG, EKG, pulse oximeter; retro and prospective.

To demonstrate the functionality of cardiac triggering, the most common sequences for cardiac imaging in MR were

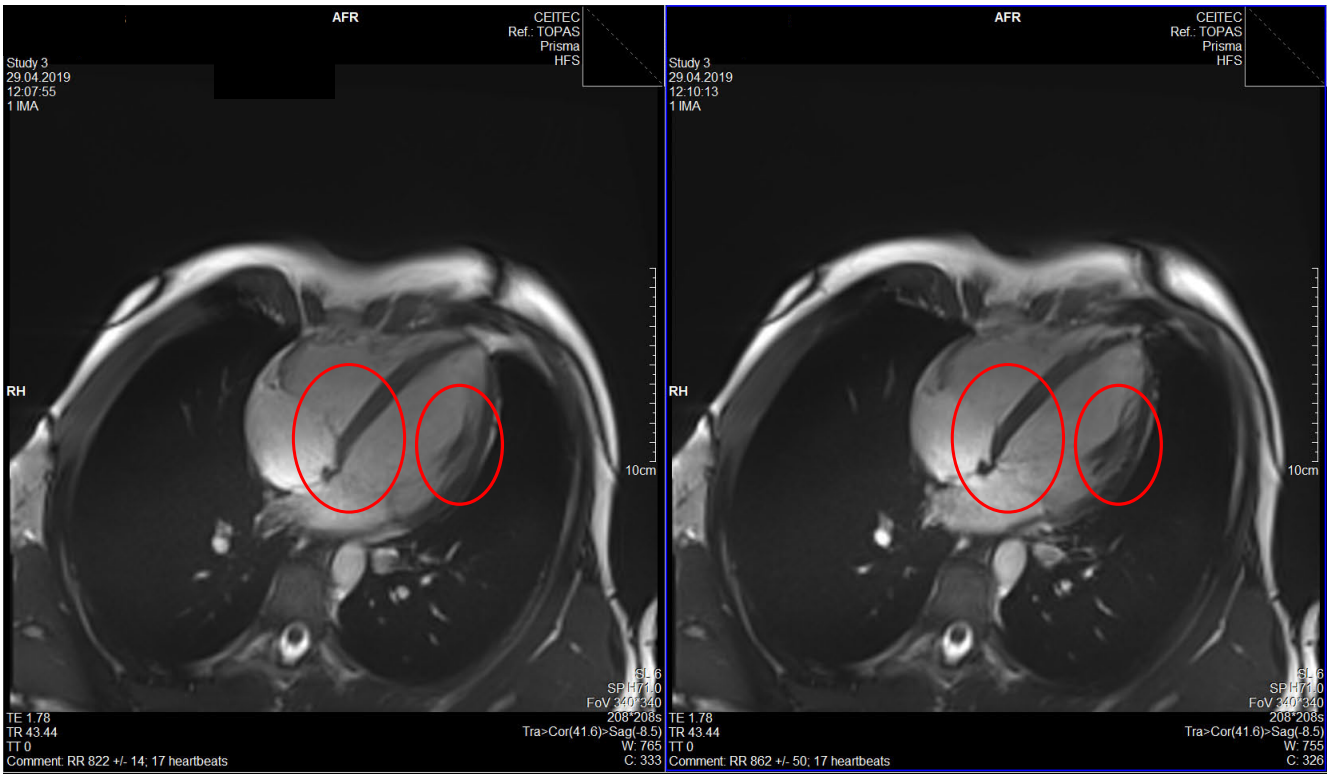

FIGURE 31. Resulting cardiac MRI of a 4-chamber view obtained using ECG (left) and SCG (right) triggering system.

used: the kinetic method - Tru FISP, and the method for detecting myocardium saturation - T1 flash, see Fig. 31 and Fig. 32 below, where ECG triggering was used on the left side and triggering using the SCG system tested on the right side.

Fig. 31 shows a scan of 4-chamber (4-cavity) T1/T2 plane of sequences of the balanced echo - Tru FISP by Siemens, Erlangen, Germany. Both images display good tissue contrast, particularly at the site of flowing blood and myocardium, without distortions at the transition site. In a 3-T device environment, the study of cardiac sections is very sensitive to movement and transition artifacts - flowing blood - left ventricle muscle; flowing blood - papillary muscles, which both ways of triggering cope well with, but still, from a medical point of view, in the SCG sequence, the image appears sharper (interventricular septum), with a higher contrast between light blood and dark muscle (especially the heart septum and papillary muscles), which may be a good guide especially for segmentation of cardiac sections.

Fig. 32 shows a study on a volunteer, natively, contrast medium not administered. T1 flash sequence measured natively - is intended to evaluate late enhancement. In the images demonstrated, there is a 2CH (2-cavity) image, where the left ventricular contour is well detectable in both triggering methods; sequences with both triggering methods are medically fit for use.

Based on the subjective evaluation of the images, Fig. 31 and Fig. 32, shown above performed by physicians, the results of the effectiveness of cardiac activity monitoring were also confirmed by cardiac triggering. It can be stated that cardiac activity monitoring is at least fully comparable with the systems used in clinical practice, which is unequivocally demonstrated by the comparison of the above-mentioned images.

TABLE 4. Results of the image quality evaluation based on BRISQUE method.

	Fig. 33		Fig. 34	
	ECG	SCG	ECG	SCG
Whole scan	44.77	44.65	43.13	43.16
Cropped scan	41.06	39.81	41.67	41.88

In addition to the subjective view of radiologists, the quality assessment of images from MRI was also carried out by software quality analysis using the Blind/Referenceless Image Spatial Quality Evaluator (BRISQUE) [83], [84]. The output of this method is a numerical quality score, which takes values from 0 (best) to 100 (worst). Quality analysis was performed for Fig. 33 and 34. The Quality Score is shown in Table 4. The results of image quality analysis show that in all cases during the cardiac triggering were achieved by the our system equivalent or better images quality.

Results presented in Table 4 show that the SCG method is equivalent to the ECG-based triggering. The quality of the scans is comparable regarding the BRISQUE method.

VI. DISCUSSION

The benefit of the system tested is the higher reliability and stability of the signal measured, without limiting the depth of the patient's inspiration (deepened inspiration, especially in

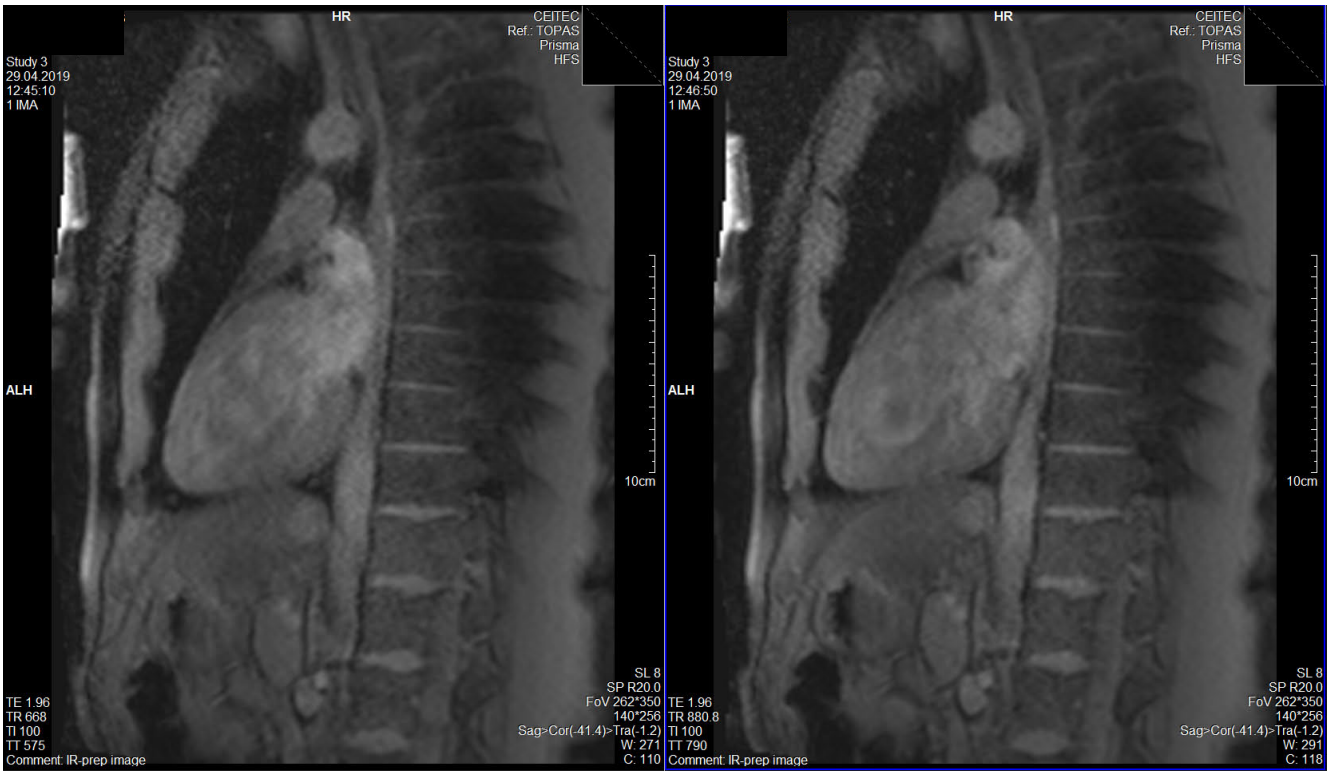

FIGURE 32. Resulting cardiac MRI in sagittal plane obtained using ECG (left) and SCG (right) triggering system.

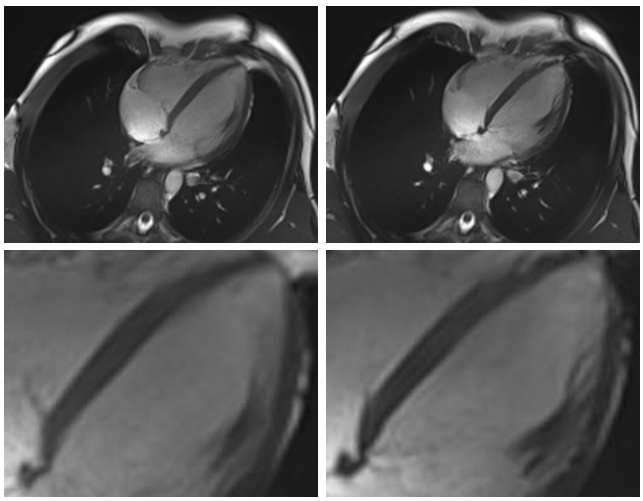

FIGURE 33. Parts selected for the objective image quality evaluation using BRISQUE (4-chamber; T1/T2 plane of sequences of the balanced echo). Left: Scan triggered by means of ECG (upper image: Whole scan; lower image: Cropped scan); Right: Scan triggered by means of SCG (upper image: Whole scan; lower image: Cropped scan).

time-consuming examinations requiring the patient to concentrate on breathing). Furthermore, it should be noted that the system tested is fully compatible with various MRI manufacturers. The test system appears to be very convenient for examinations where the emphasis is placed on continuous cardiac activity monitoring regardless of the sequence selected. For example, it is beneficial for patients with malignant arrhythmias where continuous monitoring is an essential part of patient care.

Another advantage of the system tested from the perspective of the patient, but also of the operating staff, is easier handling with the sensor itself when placing it on the body, see Fig. 7. This leads to faster preparation of the patient for examination, as there is no need to prepare the skin (shaving, degreasing, etc.) to attach the measuring electrodes. This pilot study has shown that the system tested is not dependent on the depth of inspiration. This seems to be very convenient for patients who have a problem to cooperate during the examination (small children, seniors, etc.). In systems that are currently used in clinical practice, measurements often have to be repeated. This problem is completely eliminated with the system tested. It can be assumed that thanks to the aforementioned benefits, the system tested can reduce the examination time and streamline the workflow in the workplace.

The disadvantage of the system devised is its susceptibility to the patient's movement artifacts. If the patient moves during the examination, false positive (FP) values and false negative (FN) values may occur.

The subject of further research will be usability testing for cardiac MR, neurofunctional brain imaging - diffusion tensor imaging, functional MRI, or a fluid flow detection study. Furthermore, analysis and verification of functionality in very high fields (7 T - AKH Vienna) will be conducted. Next, the collective of authors intends to focus on utilization

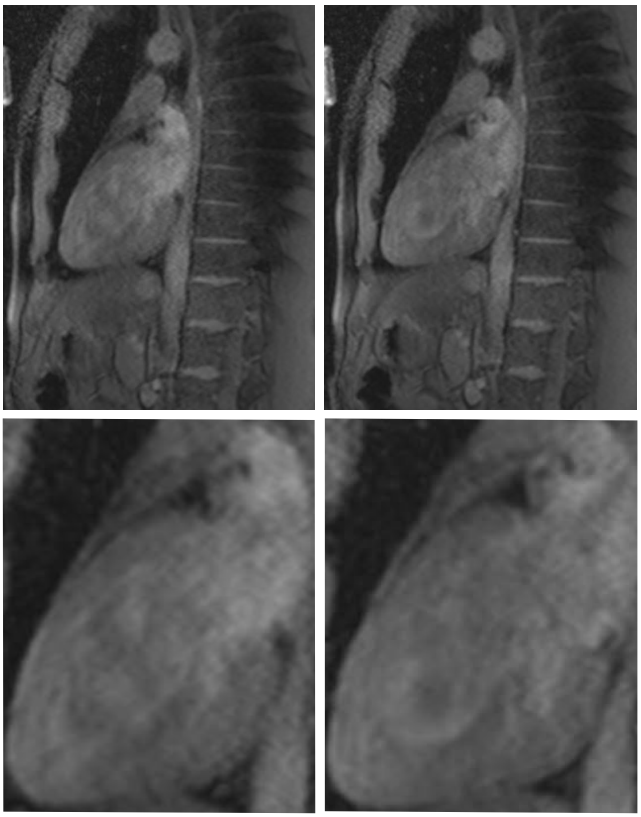

FIGURE 34. Parts selected for the objective image quality evaluation using BRISQUE (T1 flash sequence measured natively). Left: Scan triggered by means of ECG (upper image: Whole scan; lower image: Cropped scan); Right: Scan triggered by means of SCG (upper image: Whole scan; lower image: Cropped scan).

TABLE 5. Total price of the proof of concept measuring system.

Part name	Description	Price
NI cRIO-9073	Integrated Systems with Real-Time Controller	2 700 €
NI 9234	4-Channel, Sound and Vibration Input Module	2 000 €
NI 9472	8-Channel (Sourcing Output)	100 €
GRAS 40PP CPP	Free-field QC Microphone	400 €
Cables	Connecting cables	20 €
PVC 25 m	Acoustic tube	30 €
	Total price	**5 250 €**

TABLE 6. Estimated price of a series-produced measuring system.

Part	Price
Microphone	10 €
Acoustic tube	30 €
Printed cuircid board	20 €
Housing	10 €
Electronics	30 €
Total price	**100 €**

of respiratory monitoring with implementation in cardio MRI sequences.

To verify the principle of the presented device, the NI virtual instrumentation tools were used (Table 5). This equipment was chosen, because it allowed rapid prototyping of the proposed triggering system. The initial tests included the successful use of low-cost components described in Table 6. Table 7 shows the comparison of the tested systems with the commercially available systems for synchronous measurement utilized in the MRI of the research center CEITEC, Brno.

TABLE 7. The comparison of monitoring systems.

Name	Price	Measured signal
BRAINVISION - BrainAmp ExG system	∼ 40 000 €	ECG
Siemens PMU (PERU and PPU)	∼ 8 000 €	ECG, Pulse, Respiratory
Proof of concept setup	**5 300 €**	SCG
MRI PULSE OXIMETER 03-7500FO	∼ 1 500 €	Pulse
Construction cost of low-cost variant	**100 €**	SCG

VII. CONCLUSION

This pilot clinical study unambiguously confirmed the functionality of the SCG-based system tested in terms of continuous cardiac activity monitoring and the subsequent cardiac triggering. In all 18 subjects tested, cardiac activity was continuously monitored throughout the examination, regardless of the type of sequence being run. It can be stated that the SCG system tested is completely immune to all sequences tested within Siemens Prisma 3T. System functionality was verified against a commercially available ECG-based system (BRAINVISION - BrainAmp ExG system by BRAIN Product). Unfortunately, this reference system did not work reliably for a number of sequences, e.g. during a sequence of diffusion weighted echo using epitechnics, or during a sequence of 3D T2 weighted TSE ECHO - SPACE, see Chapter 5.1. For this reason, only the sections where R oscillation could be correctly detected were manually selected for the statistical analysis, so that the analysis was not distorted, see Chapter 5.2. In all 18 subjects, a mean PPV > 99 % was achieved; F1 > 99 %; SE > 99 %; ACC > 98 %; 1.96σ;< 3.5 bpm, see Table 2. Also, Cardiac Triggering functionality was confirmed by the physicians on the basis of analyzing cardiac images using the T1/T2 balanced echo sequences (Fig. 31) and the T1 flash sequence measured natively (Fig. 32).

ETHICS STATEMENT

Ref. No.: EKV-2018-010
Project Title: MR imaging sequences and protocols optimization aiming to application of new coil and pulse sequences
Proposal: 0319/2018
Investigator: Ing. Lubomir Vojtisek, Ph.D.
Organisational Unit: CEITEC

The Research Ethics Committee of Masaryk University has reviewed the application to conduct the research project as specified above and on 8 June 2018 the Committel has approved this project to be conducted. The Committee expects to be informed about any revision in the research pro-

tocols and/or informed consent form and ask to be provided a copy of the final report.

REFERENCES

[1] J. Rieber, A. Huber, I. Erhard, S. Mueller, M. Schweyer, A. Koenig, T. M. Schiele, K. Theisen, U. Siebert, S. O. Schoenberg, M. Reiser, and V. Klauss, "Cardiac magnetic resonance perfusion imaging for the functional assessment of coronary artery disease: A comparison with coronary angiography and fractional flow reserve," *Eur. Heart J.*, vol. 27, no. 12, pp. 1465–1471, Jun. 2006. doi: 10.1093/eurheartj/ehl039.

[2] H. P. Kühl, M. Schreckenberg, D. Rulands, M. Katoh, W. Schäfer, G. Schummers, A. Bücker, P. Hanrath, and A. Franke, "High-resolution transthoracic real-time three-dimensional echocardiography: Quantitation of cardiac volumes and function using semi-automatic border detection and comparison with cardiac magnetic resonance imaging," *J. Amer. College Cardiol.*, vol. 43, no. 11, pp. 2083–2090, Jun. 2004. doi: 10.1016/j.jacc.2004.01.037.

[3] L. Iles, H. Pfluger, A. Phrommintikul, J. Cherayath, P. Aksit, S. N. Gupta, D. M. Kaye, and A. J. Taylor, "Evaluation of diffuse myocardial fibrosis in heart failure with cardiac magnetic resonance contrast-enhanced T1 mapping," *J. Amer. College Cardiol.*, vol. 52, no. 19, pp. 1574–1580, Nov. 2008. doi: 10.1016/j.jacc.2008.06.049.

[4] T. Niendorf, D. K. Sodickson, G. A. Krombach, and J. Schulz-Menger, "Toward cardiovascular MRI at 7 T: Clinical needs, technical solutions and research promises," *Eur. Radiol.*, vol. 20, no. 12, pp. 2806–2816, Dec. 2010. doi: 10.1007/s00330-010-1902-8.

[5] C. Santelli, R. Nezafat, B. Goddu, W. J. Manning, J. Smink, S. Kozerke, and D. C. Peters, "Respiratory bellows revisited for motion compensation: Preliminary experience for cardiovascular MR," *Magn. Reson. Med.*, vol. 65, no. 4, pp. 1097–1102, Apr. 2011. doi: 10.1002/mrm.22687.

[6] R. Millis, *Advances in Electrocardiograms: Methods and Analysis*. Norderstedt, Germany: Books on Demand, 2012.

[7] C. Brinegar, Y. J. Wu, L. M. Foley, T. K. Hitchens, Q. Ye, C. Ho, and Z. P. Liang, "Real-time cardiac MRI without triggering, gating, or breath holding," in *Proc. 30th Annu. Int. Conf. IEEE Eng. Med. Biol. Soc.*, Aug. 2008, pp. 3381–3384. doi: 10.1109/IEMBS.2008.4649931.

[8] F. Kording, B. Schoennagel, G. Lund, F. Ueberle, C. Jung, G. Adam, and J. Yamamura, "Doppler ultrasound compared with electrocardiogram and pulse oximetry cardiac triggering: A pilot study," *Magn. Reson. Med.*, vol. 74, no. 5, pp. 1257–1265, Nov. 2015. doi: 10.1002/mrm.25502.

[9] J. M. Chia, S. E. Fischer, S. A. Wickline, and C. H. Lorenz, "Performance of QRS detection for cardiac magnetic resonance imaging with a novel vectorcardiographic triggering method," *J. Mag. Reson. Imag.*, vol. 12, no. 5, pp. 678–688, Nov. 2000. doi: 10.1002/1522-2586(200011)12:5<678::AID-JMRI4>3.0.CO;2-5.

[10] D. Stab, J. Roessler, K. O'Brien, C. Hamilton-Craig, and M. Barth, "ECG triggering in ultra-high field cardiovascular MRI," *Tomography*, vol. 2, no. 3, p. 167, Sep. 2016. doi: 10.18383/j.tom.2016.00193.

[11] G. M. Pohost and K. S. Nayak, *Handbook of Cardiovascular Magnetic Resonance Imaging*. Boca Raton, FL, USA: CRC Press, 2006.

[12] A. D. Elster, *Questions and Answers in MRI*. St. Louis, MO, USA: Washington Univ. School Med., 2018.

[13] M. S. Nacif, A. Zavodni, N. Kawel, E. Y. Choi, J. A. Lima, and D. A. Bluemke, "Cardiac magnetic resonance imaging and its electrocardiographs (ECG): Tips and tricks," *Int. J. Cardiovasc. Imag.*, vol. 28, no. 6, pp. 1465–1475, Aug. 2012. doi: 10S.1007/s10554-011-9957-4.

[14] H. Kugel, C. Bremer, M. Püschel, R. Fischbach, H. Lenzen, B. Tombach, H. Van Aken, and W. Heindel, "Hazardous situation in the MR bore: Induction in ECG leads causes fire," *Eur. Radiol.*, vol. 13, no. 4, pp. 690–694, Apr. 2003. doi: 10.1007/s00330-003-1841-8.

[15] S. Lange and Q. N. Nguyen, "Cables and electrodes can burn patients during MRI," *Nursing Manage.*, vol. 36, no. 11, p. 18, Nov. 2006. doi: 10.1097/00152193-200611000-00012.

[16] J. W. Krug, G. Rose, D. Stucht, G. Clifford, and J. Oster, "Limitations of VCG based gating methods in ultra high field cardiac MRI," *J. Cardiovascular Magn. Reson.*, vol. 15, no. 1, Jan. 2013, Art. no. W19. doi: 10.1186/1532-429X-15-S1-W19.

[17] C. J. Snyder, L. DelaBarre, G. J. Metzger, P. F. van de Moortele, C. Akgun, K. Ugurbil, and J. T. Vaughan, "Initial results of cardiac imaging at 7 tesla," *Magn. Reson. Med.*, vol. 61, no. 3, pp. 517–524, Mar. 2009. doi: 10.1002/mrm.21895.

[18] M. Becker, T. Frauenrath, F. Hezel, G. A. Krombach, U. Kremer, B. Koppers, C. Butenweg, A. Goemmel, J. F. Utting, J. Schulz-Menger, and T. Niendorf, "Comparison of left ventricular function assessment using phonocardiogram- and electrocardiogram-triggered 2D SSFP CINE MR imaging at 1.5 T and 3.0 T," *Eur. Radiol.*, vol. 20, no. 6, pp. 1344–1355, Jun. 2010. doi: 10.1007/s00330-009-1676-z.

[19] D. Abi-Abdallah, V. Robin, A. Drochon, and O. Fokapu, "Alterations in human ECG due to the MagnetoHydroDynamic effect: A method for accurate R peak detection in the presence of high MHD artifacts," in *Proc. 29th Annu. Int. Conf. IEEE Eng. Med. Biol. Soc.*, Aug. 2007, pp. 1842–1845. doi: 10.1109/IEMBS.2007.4352673.

[20] D. W. Chakeres, A. Kangarlu, H. Boudoulas, and D. C. Young, "Effect of static magnetic field exposure of up to 8 Tesla on sequential human vital sign measurements," *J. Mag. Reson. Imag.*, vol. 18, no. 3, pp. 346–352, Sep. 2003. doi: 10.1002/jmri.10367.

[21] M. Jekic, Y. Ding, R. Dzwonczyk, P. Burns, S. V. Raman, and O. P. Simonetti, "Magnetic field threshold for accurate electrocardiography in the MRI environment," *Mag. Reson. Med.*, vol. 64, no. 6, pp. 1586–1591, Dec. 2010. doi: 10.1002/mrm.22419.

[22] M. Schwartz, P. Martirosian, G. Steidle, M. Erb, B. Yang, and F. Schick, "Feasibility of real-time surface electromyographytriggered diffusion-weighted imaging for prospective imaging of spontaneous unintentional focal muscular motion in human calf musculature," in *Proc. 34th Annu. Sci. Meeting Eur. Soc. Magn. Reson. Med. Biol. (ESMRMB)*, Barcelona, Spain, Oct. 2017, pp. S83–S84.

[23] A. Babayan *et al.*, "A mind-brain-body dataset of MRI, EEG, cognition, emotion, and peripheral physiology in young and old adults," *Sci. Data*, vol. 6, Feb. 2019, Art. no. 180308. doi: 10.1038/sdata.2018.308.

[24] M. R. Borich, S. L. Wolf, A. Q. Tan, and J. A. Palmer, "Targeted neuromodulation of abnormal interhemispheric connectivity to promote neural plasticity and recovery of arm function after stroke: A randomized crossover clinical trial study protocol," *Neural Plasticity*, vol. 2018, Feb. 2018, Art. no. 9875326. doi: 10.1155/2018/9875326.

[25] H. Furby, E. Yhnell, F. Mazzaschi, J. Mole, M. Busse, A. E. Rosser, and C. Metzler-Baddeley, "E06 using 3T MRI to explore myelin breakdown in pre-symptomatic huntington's disease," Tech. Rep., 2018, doi: 10.1136/jnnp-2018-EHDN.100.

[26] *Siemens Prisma 3T MRI Scanner User Guide*. Ahmanson-Lovelace Brain Mapping Center, Los Angeles, CA, USA, 2019.

[27] *Ceitec*, Central Eur. Inst. Technol., Brno, Czechia, 2019.

[28] *Multimodal and Functional Imaging Laboratory*, Central Eur. Inst. Technol., Brno, Czechia, 2019.

[29] A. C. Larson, R. D. White, G. Laub, E. R. McVeigh, D. Li, and Simonetti, "Self-gated cardiac cine MRI," *Magn. Reson. Med.*, vol. 51, no. 1, pp. 93–102, Jan. 2004. doi: 10.1002/mrm.10664.

[30] F. Kording, J. Yamamura, G. Lund, F. Ueberle, C. Jung, G. Adam, and B. P. Schoennagel, "Doppler ultrasound triggering for cardiovascular MRI at 3T in a healthy volunteer study," *Magn. Reson. Med. Sci.*, vol. 16, no. 2, pp. 98–108, Apr. 2017. doi: 10.2463/mrms.mp.2015-0104.

[31] T. Niendorf, L. Winter, and T. Frauenrath, "Electrocardiogram in an MRI environment: Clinical needs, practical considerations, safety implications, technical solutions and future directions," in *Advances in Electrocardiograms-Methods and Analysis*. 2012.

[32] S. E. Fischer, S. A. Wickline, and C. H. Lorenz, "Novel real-time R-wave detection algorithm based on the vectorcardiogram for accurate gated magnetic resonance acquisitions," *Magn. Reson. Med.*, vol. 42, no. 2, pp. 361–370, Aug. 1999. doi: 10.1002/(SICI)1522-2594(199908)42:2<361::AID-MRM18>3.0.CO;2-9.

[33] L. Axel and M. A. Toms, "Clinical cardiac magnetic resonance imaging techniques," in *Cardiovascular Magnetic Resonance Imaging*. 2019, pp. 17–50. doi: 10.1007/978-1-4939-8841-9_2.

[34] N. Spicher, M. Kukuk, S. Maderwald, and M. E. Ladd, "Initial evaluation of prospective cardiac triggering using photoplethysmography signals recorded with a video camera compared to pulse oximetry and electrocardiography at 7T MRI," *Biomed. Eng. Online*, vol. 15, no. 1, p. 126, Nov. 2016. doi: 10.1186/s12938-016-0245-3.

[35] N. Spicher, "Cardiac activity measurement from video signals of the human skin in ultrahigh-field magnetic resonance imaging," *Informatik*, vol. 2016, pp. 1–6, 2016.

[36] A. C. Larson, P. Kellman, A. Arai, G. A. Hirsch, E. McVeigh, D. Li, and O. P. Simonetti, "Preliminary investigation of respiratory self-gating for free-breathing segmented cine MRI," *Magn. Reson. Med.*, vol. 53, no. 1, pp. 159–168, Jan. 2005. doi: 10.1002/mrm.20331.

[37] E. Heijman, W. de Graaf, P. Niessen, A. Nauerth, G. van Eys, L. de Graaf, K. Nicolay, and G. J. Strijkers, "Comparison between prospective and retrospective triggering for mouse cardiac MRI," *NMR Biomed.*, vol. 20, no. 4, pp. 439–447, Jun. 2007. doi: 10.1002/nbm.1110.

[38] X. Hu, T. H. Le, T. Parrish, and P. Erhard, "Retrospective estimation and correction of physiological fluctuation in functional MRI," *Mag. Reson. Med.*, vol. 34, no. 2, pp. 201–212, Aug. 1995. doi: 10.1002/mrm.1910340211.

[39] G. M. Nijm, A. V. Sahakian, S. Swiryn, J. C. Carr, J. J. Sheehan, and A. C. Larson, "Comparison of self-gated cine MRI retrospective cardiac synchronization algorithms," *J. Mag. Reson. Imag.*, vol. 28, no. 3, pp. 767–772, Sep. 2008. doi: 10.1002/jmri.21514.

[40] H. Mandelkow, D. Brandeis, and P. Boesiger, "Good practices in EEG-MRI: The utility of retrospective synchronization and PCA for the removal of MRI gradient artefacts," *Neuroimage*, vol. 49, no. 3, pp. 2287–2303, 2010. doi: 10.1016/j.neuroimage.2009.10.050.

[41] M. Gutberlet, K. Schwinge, P. Freyhardt, B. Spors, M. Grothoff, T. Denecke, L. Lüdemann, R. Noeske, T. Niendorf, and R. Felix, "Influence of high magnetic field strengths and parallel acquisition strategies on image quality in cardiac 2D CINE magnetic resonance imaging: Comparison of 1.5 T vs. 3.0 T.," *Eur. Radiol.*, vol. 15, no. 8, pp. 1586–1597, Aug. 2005. doi: 10.1007/s00330-005-2768-z.

[42] F. von Knobelsdorff-Brenkenhoff, T. Frauenrath, M. Prothmann, M. A. Dieringer, F. Hezel, W. Renz, K. Kretschel, T. Niendorf, and J. Schulz-Menger, "Cardiac chamber quantification using magnetic resonance imaging at 7 tesla—A pilot study," *Eur. Radiol.*, vol. 20, no. 12, pp. 2844–2852, Dec. 2010. doi: 10.1007/s00330-010-1888-2.

[43] T. Frauenrath, F. Hezel, W. Renz, and T. de Geyer d'Orth, M. Dieringer, F. von Knobelsdorff-Brenkenhoff, M. Prothmann, J. S. Menger, and T. Niendorf, "Acoustic cardiac triggering: A practical solution for synchronization and gating of cardiovascular magnetic resonance at 7 tesla," *J. Cardiovascular Magn. Reson.*, vol. 12, no. 1, p. 67, Nov. 2010. doi: 10.1186/1532-429X-12-67.

[44] R. Hoffmann, S. von Bardeleben, J. D. Kasprzak, A. C. Borges, F. ten Cate, C. Firschke, S. Lafitte, N. Al-Saadi, S. Kuntz-Hehner, G. Horstick, C. Greis, M. Engelhardt, J. L. Vanoverschelde, H. Becher, and C. Greis, "Analysis of regional left ventricular function by cineventriculography, cardiac magnetic resonance imaging, and unenhanced and contrast-enhanced echocardiography: A multicenter comparison of methods," *J. Amer. College Cardiol.*, vol. 47, no. 1, pp. 121–128, Jan. 2006. doi: 10.1016/j.jacc.2005.10.012.

[45] T. Frauenrath, F. Hezel, U. Heinrichs, S. Kozerke, J. F. Utting, M. Kob, C. Butenweg, T. Niendorf, and T. Niendorf, "Feasibility of cardiac gating free of interference with electro-magnetic fields at 1.5 tesla, 3.0 Tesla and 7.0 tesla using an MR-stethoscope," *Investigative Radiol.*, vol. 44, no. 9, pp. 539–547, Sep. 2009. doi: 10.1097/RLI.0b013e3181b4c15e.

[46] A. C. S. Brau, C. T. Wheeler, L. W. Hedlund, and G. A. Johnson, "Fiber-optic stethoscope: A cardiac monitoring and gating system for magnetic resonance microscopy," *Magn. Reson. Med.*, vol. 47, no. 2, pp. 314–321, Feb. 2002. doi: 10.1002/mrm.10049.

[47] F. Tobias, S. Kozerke, F. Henzel, and T. Niendorf, "The MR-stethoscope: Safe cardiac gating free of interference with electro-magnetic fields at 1.5 T, 3.0 T and 7.0 T," *J. Cardiovascular Mag. Reson.*, vol. 11, no. 1, 2009, Art. no. O78. doi: 10.1186/1532-429X-11-S1-O78.

[48] S. G. van Elderen, M. J. Versluis, J. J. Westenberg, H. Agarwal, N. B. Smith, M. Stuber, A. de Roos, and A. G. Webb, "Right coronary MR angiography at 7 T: A direct quantitative and qualitative comparison with 3 T in young healthy volunteers," *Radiology*, vol. 257, no. 1, pp. 254–259, Oct. 2010. doi: 10.1148/radiol.100615.

[49] S. Maderwald, S. Orzada, Z. Lin, L. C. Schafer, A. K. Bitz, O. Kraff, and K. Nassenstein, "7 tesla cardiac imaging with a phonocardiogram trigger device," in *Proc. Int. Soc. Magn. Reson. Med.*, Montreal, QC, Canada, vol. 19, May 2011, p. 1322.

[50] T. Frauenrath, S. Kozerke, P. Boesiger, and T. Niendorf, "Cardiac gating free of interference with electro-magnetic fields at 1.5 T, 3.0 T and 7.0 T," in *Proc. Annu. Meeting Int. Soc. Magn. Reson. Med.*, Toronto, ON, Canada, May 2008, p. 207.

[51] K. Nassenstein, S. Orzada, L. Haering, A. Czylwik, M. Zenge, H. Eberle, T. Schlosser, O. Bruder, E. Müller, M. E. Ladd, and S. Maderwald, "Cardiac MRI: Evaluation of phonocardiogram-gated cine imaging for the assessment of global und regional left ventricular function in clinical routine," *Eur. Radiol.*, vol. 22, no. 3, pp. 559–568, Mar. 2012. doi: 10.1007/s00330-011-2279-z.

[52] B. Hiba, N. Richard, M. Janier, and P. Croisille, "Cardiac and respiratory double self-gated cine MRI in the mouse at 7 T," *Magn. Reson. Med.*, vol. 55, no. 3, pp. 506–513, Mar. 2006. doi: 10.1002/mrm.20815.

[53] J. M. Rubin, J. B. Fowlkes, M. R. Prince, R. T. Rhee, and T. L. Chenevert, "Doppler US gating of cardiac MR imaging," *Academic Radiol.*, vol. 7, no. 12, pp. 1116–1122, Dec. 2000. doi: 10.1016/S1076-6332(00)80065-3.

[54] D. A. Feinberg, D. Giese, D. A. Bongers, S. Ramanna, M. Zaitsev, M. Markl, and M. Gunther, "Hybrid ultrasound MRI for improved cardiac imaging and real-time respiration control," *Magn. Reson. Med.*, vol. 63, no. 2, pp. 290–296, Feb. 2010. doi: 10.1002/mrm.22250.

[55] X. Cheng, H. Li, Y. Chen, B. Luo, X. Liu, W. Liu, H. Xu, and X. Yang, "Ultrasound-triggered phase transition sensitive magnetic fluorescent nanodroplets as a multimodal imaging contrast agent in rat and mouse model," *PLoS ONE*, vol. 8, no. 12, Dec. 2013, Art. no. e85003. doi: 10.1371/journal.pone.0085003.

[56] S. Vitek, A. Ezion, and D. Freundlich, U.S. Patent 6 735 461, 2004.

[57] A. Rengle, L. Baboi, H. Saint-Jalmes, R. Sablong, and O. Beuf, "Optical cardiac and respiratory device for synchronized MRI on small animal," in *Proc. 29th Annu. Int. Conf. IEEE Eng. Med. Biol. Soc.*, Aug. 2007, pp. 2046–2049. doi: 10.1109/IEMBS.2007.4352722.

[58] M. Fajkus, J. Nedoma, R. Martinek, V. Vasinek, H. Nazeran, and P. Siska, "A non-invasive multichannel hybrid fiber-optic sensor system for vital sign monitoring," *Sensors*, vol. 17, no. 1, p. 111, Jan. 2017. doi: 10.3390/s17010111.

[59] J. Nedoma, M. Fajkus, M. Novak, N. Strbikova, V. Vasinek, H. Nazeran, J. Vanus, F. Perecar, and R. Martinek, "Validation of a novel fiber-optic sensor system for monitoring cardiorespiratory activities during MRI examinations," *Adv. Elect. Electron. Eng.*, vol. 15, no. 3, pp. 536–543, Sep. 2017. doi: 10.15598/aeee.v15i3.2194.

[60] Ł. Dziuda, "Fiber-optic sensors for monitoring patient physiological parameters: A review of applicable technologies and relevance to use during magnetic resonance imaging procedures," *J. Biomed. Opt.*, vol. 20, no. 1, Jan. 2015, Art. no. 010901. doi: 10.1117/1.JBO.20.1.010901.

[61] J. Nedoma, M. Fajkus, R. Martinek, and V. Vasinek, "Analysis of non-invasive FBG sensor for monitoring patient vital signs during MRI," *Proc. SPIE*, vol. 10440, Oct. 2017, Art. no. 104400H. doi: 10.1117/12.2277399.

[62] *Reconfigurable Embedded Chassis with Integrated Intelligent RealTime Controller for CompactRIO*, document NI cRIO-9072/9073/9074, Nat. Instrum., Austin, TX, USA.

[63] S. H. Lee, H. C. Kim, and K. S. Jung, "Atomic force microscopy using optical pickup head to measure cantilever displacement," *Int. J. Precis. Eng. Manuf.*, vol. 12, no. 5, pp. 913–915, Oct. 2011. doi: 10.1007/s12541-011-0122-8.

[64] T. A. Ishola, A. Yahya, A. R. M. Shariff, and S. A. A. Aziz, "A novel variable rate pneumatic fertilizer applicator," *Instrum. Sci. Technol.*, vol. 42, no. 4, pp. 369–384, Mar. 2014. doi: 10.1080/10739149.2013.879663.

[65] R. Martinek, J. Brablik, L. Soustek, J. Kolarik, M. Fajkus, J. Nedoma, and R. Kahankova, "A comparison of probes based on Bragg grating sensor and microphones for heart sounds measurement," *Proc. SPIE*, vol. 10801, Oct. 2018, Art. no. 108010G. doi: 10.1117/12.2325744.

[66] R. Martinek, R. Kahankova, J. Nedoma, M. Fajkus, and M. Skacel, "Comparison of the LMS, NLMS, RLS, and QR-RLS algorithms for vehicle noise suppression," in *Proc. 10th Int. Conf. Comput. Modeling Simulation*, Jan. 2018, pp. 23–27. doi: 10.1145/3177457.3177502.

[67] C. J. Peters, R. B. Miles, R. A. Burns, P. M. Danehy, B. F. Bathel, and G. S. Jones, "Femtosecond laser tagging characterization of a sweeping jet actuator operating in the compressible regime," in *Proc. 32nd AIAA Aerodyn. Meas. Technol. Ground Test. Conf.*, Jun. 2016, p. 3248. doi: 10.2514/6.2016-3248.

[68] *Datasheet, NI 9250 With BNC*, Nat. Instrum., Austin, TX, USA, 2017.

[69] *Datasheet, NI 9472*, Nat. Instrum., Austin, TX, USA, 2019.

[70] C. Elliott, V. Vijayakumar, W. Zink, and R. Hansen, "National instruments LabVIEW: A programming environment for laboratory automation and measurement," *J. Assoc. Lab. Automat.*, vol. 12, no. 1, pp. 17–24, Feb. 2007. doi: 10.1016/j.jala.2006.07.012.

[71] R. Martinek, R. Kahankova, P. Bilik, J. Nedoma, M. Fajkus, and M. Skacel, "Speech signal processing using microphones NI 9234 and LabVIEW," in *Proc. 10th Int. Conf. Comput. Modeling Simulation*, Jan. 2018, pp. 9–13. doi: 10.1145/3177457.3177501.

[72] R. Martinek, M. Kelnar, P. Koudelka, J. Vanus, P. Bilik, P. Janku, H. Nazeran, and J. Zidek, "A novel LabVIEW-based multi-channel non-invasive abdominal maternal-fetal electrocardiogram signal generator," *Physiol. Meas.*, vol. 37, no. 2, 238, Feb. 2016. doi: 10.1088/0967-3334/37/2/238.

[73] O. T. Inan, P. F. Migeotte, K. S. Park, M. Etemadi, K. Tavakolian, R. Casanella, J. Zanetti, J. Tank, I. Funtova, G. K. Prisk, and M. Di Rienzo, "Ballistocardiography and seismocardiography: A review of recent advances," *IEEE J. Biomed. Health Informat.*, vol. 19, no. 4, pp. 1414–1427, Jul. 2015. doi: 10.1109/JBHI.2014.2361732.
[74] A. Dinh, Y. Choi, and S.-B. Ko, "A heart rate sensor based on seismocardiography for vital sign monitoring systems" in *Proc. 24th Can. Conf. Elect. Comput. Eng. (CCECE)*, Niagara Falls, ON, Canada, May 2011, pp. 665–668. doi: 10.1109/CCECE.2011.6030536.
[75] J. M. Zanetti and K. Tavakolian, "Seismocardiography: Past, present and future," in *Proc. 35th Annu. Int. Conf. IEEE Eng. Med. Biol. Soc. (EMBC)*, Jul. 2013, pp. 7004–7007. doi: 10.1109/EMBC.2013.6611170.
[76] C. A. Wick, O. T. Inan, P. Bhatti, and S. Tridandapani, "Relationship between cardiac quiescent periods derived from seismocardiography and echocardiography," in *Proc. 37th Annu. Int. Conf. IEEE Eng. Med. Biol. Soc. (EMBC)*, Aug. 2015, pp. 687–690, doi: 10.1109/EMBC.2015.7318455.
[77] *BrainAmp, Operating and Reference Manual for Use in a Laboratory Environment, Brain Products*, 2016.
[78] J. Yao, S. Tridandapani, W. F. Auffermann, C. A. Wick, and P. T. Bhatti, "An adaptive seismocardiography (SCG)-ECG multimodal framework for cardiac gating using artificial neural networks," *IEEE J. Transl. Eng. Health Med.*, vol. 6, Art. no. 1900611, 2018. doi: 10.1109/JTEHM.2018.2869141.
[79] R. Durichen, K. D. Verma, S. Y. Yee, T. Rocznik, P. Schmidt, J. Bödecker, and C. Peters, "Prediction of electrocardiography features points using seismocardiography data: A machine learning approach," in *Proc. ACM Int. Symp. Wearable Comput.*, Oct. 2018, pp. 96–99. doi: 10.1145/3267242.3267283.
[80] M. J. Tadi, E. Lehtonen, T. Koivisto, M. Pänkäälä, A. Paasio, and M. Teras, "Seismocardiography: Toward heart rate variability (HRV) estimation," in *Proc. IEEE Int. Symp. Med. Meas. Appl. (MeMeA)*, May 2015, pp. 261–266. doi: 10.1109/MeMeA.2015.7145210.
[81] R. Martinek, R. Kahankova, J. Jezewski, R. Jaros, J. Mohylova, M. Fajkus, J. Nedoma, P. Janku, and H. Nazeran, "Comparative effectiveness of ICA and PCA in extraction of fetal ECG from abdominal signals: Toward non-invasive fetal monitoring," *Front. Physiol.*, vol. 9, p. 648, May 2018, doi: 10.3389/fphys.2018.00648.
[82] J. M. Bland and D. G. Altman, "Measuring agreement in method comparison studies," *Stat. Methods Med. Res.*, vol. 8, no. 2, pp. 135–160, Jun. 1999, doi: 10.1177/096228029900800204.
[83] A. Mittal, A. K. Moorthy, and A. C. Bovik, "No-reference image quality assessment in the spatial domain," *IEEE Trans. Image Process.*, vol. 21, no. 12, pp. 4695–4708, Dec. 2012. doi: 10.1109/TIP.2012.2214050.
[84] A. Mittal, A. K. Moorthy, and A. C. Bovik, "Referenceless image spatial quality evaluation engine," in *Proc. 45th Asilomar Conf. Signals, Syst. Comput.*, vol. 38, Nov. 2011, pp. 53–54.

RADEK MARTINEK was born in Czech Republic, in 1984. He received the master's degree in information and communication technology from the VSB-Technical University of Ostrava, in 2009. He has been a Research Fellow, since 2012. In 2014, he successfully defended his dissertation thesis titled "The Use of Complex Adaptive Methods of Signal Processing for Refining the Diagnostic Quality of the Abdominal Fetal Electrocardiogram." He became an Associate Professor of Technical Cybernetics, in 2017, after defending the habilitation thesis titled "Design and Optimization of Adaptive Systems for Applications of Technical Cybernetics and Biomedical Engineering Based on Virtual Instrumentation." He has been an Associate Professor at VSB-Technical University of Ostrava, since 2017. His current research interests include digital signal processing (linear and adaptive filtering, soft computing—artificial intelligence and adaptive fuzzy systems, non-adaptive methods, biological signal processing, and digital processing of speech signals); wireless communications (software-defined radio); power quality improvement. He has published more than 200 journal and conference articles in his research areas.

JINDRICH BRABLIK was born in 1991. He graduated from the Faculty of Electrical Engineering and Computer Science, VSB-Technical University of Ostrava. The field of study was biomedical technician for bachelor's studies and information and control systems for master's studies. He is currently pursuing the Ph.D. degree in technical cybernetics with the VSB-Technical University of Ostrava, where he focuses on virtual instrumentation and signal processing of physiological signals.

JAKUB KOLARIK was born in Ostrava, Czech Republic, in 1992. He received the bachelor's and the master's degrees in control and information systems from the Department of Cybernetics and Biomedical Engineering, VSB-Technical University of Ostrava, in 2014 and 2016, respectively. He is currently pursuing the Ph.D. degree in technical cybernetics.

MARTINA LADROVA was born in Ostrava, Czech Republic, in 1994. She received the master's degree from the Faculty of Electrical Engineering and Computer Science, VSB-Technical University of Ostrava, in 2018, where she is currently pursuing the Ph.D. degree. Her research interest includes digital signal processing, especially biological signal processing.

JAN NEDOMA was born in Czech Republic, in 1988. He has been an Assistant Professor at the VSB-Technical University of Ostrava, since 2016. His current research interests include fiber-optic sensors in traffic, civil engineering, and biomedical applications.

RENE JAROS was born in Ostrava, Czech Republic, in 1992. He graduated from the Faculty of Electrical Engineering and Computer Science, VSB-Technical University of Ostrava, in 2015, where he is currently pursuing the Ph.D. degree in technical cybernetics. In 2015, he wrote a Bachelor's thesis, which deals with transformation methods of 12-lead ECG to VCG, and in 2017, he wrote a Diploma thesis, which deals with non-adaptive methods of fetal ECG signal processing. His research interest includes fECG extraction by using hybrid methods.

LUKAS SOUSTEK was born in Karvina, Czech Republic, in 1991. He received the bachelor's and the master's degrees in control and information systems from the Department of Cybernetics and Biomedical Engineering, VSB-Technical University of Ostrava, in 2014 and 2016, respectively. He is currently pursuing the Ph.D. degree in technical cybernetics.

RADANA KAHANKOVA was born in Opava, Czech Republic, in 1991. She received the bachelor's and the master's degrees in biomedical engineering from the Department of Cybernetics and Biomedical Engineering, VSB-Technical University of Ostrava, in 2014 and 2016, respectively. She is currently pursuing the Ph.D. degree in technical cybernetics. Her current research interest includes improving the quality of electronic fetal monitoring.

MARCEL FAJKUS was born in Czech Republic, in 1987. He has been an Assistant Professor at the VSB-Technical University of Ostrava, since 2016. His current research interests include fiber Bragg sensors and distributed systems in traffic, civil engineering, and biomedical applications.

LUBOMIR VOJTISEK received the Ph.D. degree in measurement from the Faculty of Electrical Engineering and Information Technology, Slovak Technical University. He is a Researcher and Technical Specialist Member of the Multi-modal and Functional Neuroimaging Research Group. He is currently a Postdoctoral Research Fellow.

PAVLA HANZLIKOVA is currently with the Clinic of Imaging Methods of Faculty Hospital in Ostrava and deals with interventional neuroradiology, MR spectroscopy, and interventional applications of 3D image.

PETR KRUPA was born in 1954. He graduated from the Faculty of Medicine, Masaryk University, Brno. At the Clinic of Imaging Methods of Faculty Hospital in Ostrava (where he is a Head) and the Faculty of Medicine, Masaryk University, Brno, deals with interventional neuroradiology, MR spectroscopy, interventional applications of 3D image, and operating simulators.